Sewage Sludge Valorization: Biochar Production for Enhanced Adsorption of Contaminants

ANDY KOFI AGOE, Chemical and Material Engineering

Submitted in fulfillment of the requirements
for the degree of Master of Science
in Chemical Engineering and Materials Science

School of Engineering and Digital Sciences
Department of Chemical Engineering and Materials Science
Nazarbayev University

53 Kabanbay Batyr Avenue

Kazakhstan, 010000

Supervisors: Stavros G. Poulopoulos

Dhawal Shah

Yerbol Sarbassov

April 2024

DECLARATION

I hereby declare that this manuscript, entitled "**Sewage Sludge Valorization: Biochar Production for Enhanced Adsorption of Contaminants**," is the result of my own work except for quotations and citations, which have been duly acknowledged.

I also declare that, to the best of my knowledge and belief, it has not been previously or concurrently submitted, in whole or in part, for any other degree or diploma at Nazarbayev University or any other national or international institution.

Name: **Andy Kofi Agoe**

Date: **01/05/24**

Abstract

Municipal sewage sludge (SS) from wastewater treatment has attracted much interest from the agriculture and energy sectors. However, concerns about harmful contaminants in sewage sludge limit its direct use in developed countries. Alternatively, a thermochemical conversion process such as pyrolysis of SS produces several value-added products, including bio-oil and a stabilized form of pyrolytic residuals with a large specific surface area and functional groups. This study examined the effects of pyrolysis temperature (500 ^{o}C, 650 ^{o}C, and 850 ^{o}C) and SS particle size (S_1: 800 - 1000 µm, S_2: 400 - 800 µm, S_3: 100 - 400 µm, S_4: ≤ 100 µm) on the derived biochar's yield and its methylene blue and mercury adsorption capacity. The adsorption capacity and kinetics results were used to identify the best thermal treatment conditions for the SS. Irrespective of the particle size at a pyrolysis temperature of 500 ^{o}C, the SS-derived biochar followed the second-order adsorption kinetics. SS-derived biochar of 100 - 400 µm particle size was identified as a promising adsorbent due to its high adsorption capacity for methylene blue and a comparable initial adsorption and desorption rate constant based on the Elovich model. Further alkali treatment (Biochar: NaOH = 3:4) of 100 - 400 µm particle size enhanced the specific surface area of the biochar from 27.5 m^2/g to 144.27 m^2/g and increased the adsorption capacity of methylene blue and mercury to 35 mg/g and 36 mg/g respectively. These SS-based adsorbents are cost-effective and have a very high methylene blue and mercury adsorption capacity, serving as a beneficial modifier adsorbent. This advantage is poised to refine parameters in sewage sludge preparation before and after pyrolysis, offering a dependable material for engineering applications.

Acknowledgment

I am deeply grateful to God and Nazarbayev University for allowing me to undertake this scientific adventure. I sincerely thank God for His divine direction and sustenance.

Also, I profoundly thank Prof. Stavros Poulopoulos, whose mentorship has been essential over the last two years. His leadership and dedication as a scientist have been an ongoing source of encouragement.

I also want to thank my co-supervisors, Prof. Dhawal Shah and Prof. Yerbol Sarbassov, for their unflinching assistance throughout the experiment and paper assessment—my heartfelt thanks to Professor Dhawal Shah for his collaborative efforts and encouragement.

Finally, I want to thank my parents, Rosemond Agoe and Peter Agoe, and my siblings, Beatrice and Nathaniel, my little cousins, and all my friends for their continuous motivation, prayers, and encouragement throughout my master's studies program at Nazarbayev University.

I end with my local dialect, “Medasi, Onyankopɔn Nhyira wo,” translated into English as Thank you and God bless you all.

Table of Contents

Abstract **3**

Acknowledgment **4**

List of Abbreviations & Symbols **7**

List of Figures **8**

List of Tables **10**

Chapter 1 – Introduction 11

1.1 Overview of Sewage Sludge Volarization: Biochar Production for Enhanced Adsorption of Contaminants 11

1.2 Aims 13

1.3 Objectives 13

1.4 The Novelty of the Research 14

1.5 Thesis Organization 14

Chapter 2 –Literature Review 16

2.1 Thermochemical Conversion 16

2.2 Sewage Sludge as Adsorbent 17

2.3 Adsorption Process 20

2.4 Methylene Blue (MB) Adsorption 21

2.5 Mercury Adsorption 21

Chapter 3–Materials and Methods 22

3.1 Preparation of Municipal Sewage Sludge (SS) 22

3.2 Pyrolysis in a Horizontal Quartz Tube Reactor 22

3.3 Modification of the Sludge-derived Biochar 23

3.4 Experimental Procedure 24

3.4.1 Methylene Blue Adsorption Kinetics 24

3.4.2 Mercury Adsorption 24

3.5 Material Characterization 26

Chapter 4 –Results and Discussion 27

4.1 Effects of Pyrolysis Temperature on Sludge-derived Biochar 27

4.2 Characterization of Sewage Sludge-derived Biochar 28

4.2.1 Heavy Metals in SS and Sewage Sludge-derived Biochar 28

4.2.2 Surface Morphology of Sludge-derived Biochar and Modified Biochar 29
4.2.3 Specific Surface Area of the SS-derived Biochar and Modified Biochar at Different Temperatures 30
4.2.4 Structural Characterization of SS, Sewage Sludge Biochar, and Modified Biochar 31
4.3 Batch Adsorption Studies of Methylene Blue 33
4.3.1 MB Adsorption onto Different Particle Sizes of Sludge-derived Biochar 33
4.3.2 Effect of Methylene Blue Concentration on Adsorbent Mass 34
4.3.3 MB Adsorption Kinetics of Different Particle Sizes of Sewage Sludge-Derived Biochar 35
4.3.3.1 Pseudo First-Order and Pseudo Second-Order Model……..….35
4.3.3.2 Webber Moris Model 36
4.3.3.3 Elovich Model……..……..37
4.4 Effect of Adsorbent (S_3:100 – 400 µm) Dosage in MB Solution 38
4.5 Influence of Pyrolysis Temperature and Alkali Activation on Adsorption……...38
4.5.1 Methylene Blue Removal……....38
4.5.2 Mercury Removal……...39
4.6 Possible Mechanism of MB and Hg^{+2} Adsorption onto Sludge-derived Biochar and Modified Biochar 40
4.6 Comparative Study with Other Adsorbent Materials 41
Chapter 5 – Conclusion 43
References 44
APPENDICES 56

List of Abbreviations & Symbols

C	Constant related to the effect of the thickness of the boundary layer
C_o	Initial concentration
Ct	Final Concentration
FTIR	Fourier Transform infra-red spectroscopy
Hg	Mercury (II) from Hg $(NO_3)_2$. H_2O
k_1	Pseudo-first-order adsorption rate constant
k_2	Pseudo second-order adsorption rate constant
k_d	Intraparticle diffusion rate
MS_3-500	Particle size of sludge-derived biochar modified at 500 ◦C
MS_3-650	Particle size of sludge-derived biochar modified at 650 ◦C
MS_3-800	Particle size of sludge-derived biochar modified at 800 ◦C
MB	Methylene Blue
NaOH	Sodium hydroxide
pH	Power of hydrogen
Q_e	Adsorption amount at equilibrium
Q_t	Adsorption amount at a specific time
R	Correlation coefficients
rpm	Revolutions per minutes
SS	Municipal Sewage Sludge
S_1	Sludge-derived biochar of particle size 800 µm -1000 µm
S_2	Sludge-derived biochar of particle size 400 µm - 800 µm
S_3	Sludge-derived biochar of particle size 100 µm - 400 µm
S_4	Sludge-derived biochar of particle size d ≤ 100 µm
S_n-500	Particle size of sludge-derived biochar pyrolyzed at 500 where n=1,2,3,4
S_n-650	Particle size of sludge-derived biochar pyrolyzed at 650 where n=1,2,3,4
S_n-800	Particle size of sludge-derived biochar pyrolyzed at 800 where n=1,2,3,4
t	time
UV-Vi's	Ultra-violet visible spectroscopy
WHO	World health organization

List of Figures

Fig. 1 Integrated Circular Economy Strategy for Municipal Sewage Sludge……..….13
Fig. 2 Potential biomass to bioenergy pathways via thermochemical conversion……17
Fig. 3 Chemical nature of MB 21
Fig. 4 Schematic Diagram of a Horizontal Quartz Tube Reactor…….23
Fig. 5 The calibration plot used for MB quantification on UV-Vis..... 24
Fig. 6 Schematic Diagram of Mercury Thermal Decomposition Experimental System……25
Fig. 7 Effect of Different SS Particle Sizes on the Biochar Yield (%) at Different Pyrolysis Temperatures..... 28
Fig. 8 Total amount of Fe^{+2}, Mn^{+2}, and Zn^{+2} in the Different Particle Sizes of Sewage Sludge at 500, 650, and 800 °C. 29
Fig 9 Surface Morphology of Sludge-derived biochar (A, B, E) and modified biochar (C, D, F). 30
Fig. 10 Structure Characterization of Sewage Sludge (SS), Sludge-derived Biochar (S_3), and Modified Sludge-derived Biochar (MS_3) for S_3-Sized Particles at 500 °C, 650 °C and 800 °C .. 32
Fig. 11 MB Adsorption Capacity versus Time 33
Fig. 12 Adsorption Capacity versus Initial MB concentration. 34
Fig. 13 Nonlinear 1st Order(A) and 2nd order(B) Kinetic fit for MB Adsorption onto Sludge-derived Biochar of Different Particle Sizes 35
Fig.14 Intra-particle Diffusion of MB Adsorption on Sludge-derived Biochar of Different Particle Sizes..... 36
Fig.15 Elovich Model of MB Adsorption on Sludge-derived Biochar of Different Particle Sizes…….…….37
Fig. 16 Effect of Adsorbent Dosage 38
Fig 17. Methylene blue Adsorption Capacity with Time 39
Fig 18. Mercury Adsorption Capacity with Time..... 40
Fig. 19 Possible Interactions of Methylene Blue (MB) and Mercury (Hg^{+2}) Adsorption onto Biochar Derived from Sludge And Modified Biochar……...41
Fig 20. Comparison of Adsorption Capacity with other adsorbent 42

Appendices Chapter 3……56
Fig A1. Location of Sewage Sludge Treatment Facility……56
Fig A2. Flowchart of Preparation of Municipal Sewage Sludge 57
Fig A3 Flowchart of Synthesis of Modified Biochar(MS_3)..... 57
Fig A4 Shows the Operation of the Mercury Analyzer 60
Appendices Chapter 4……61
Fig B2 Physical Nature of sewage sludge-derived biochar pyrolyzed at 500 °C, 650 °C and 800 °C During Initial MB Adsorption and at the equilibrium stage..... 61
Fig. B3 Adsorption Capacity of SS-derived Biochar at 650 °C (B) and at 800 °C (C) versus Time……...61

List of Tables

Table 1. Comparison of Different Modifications of Municipal Sewage Sludge and its Specific S_{BET} Area…….….19

Table 2. Adsorption Capacity of other Adsorbents in different Pollutants ……..…….20

Table 3. Pore Structure Parameter of the Particle size (S_3) of Sludge-derived Biochar and NaOH-Modified biochar at Different Temperatures...……..…30

Appendices Chapter 3……...58

Table A6 Assay of Chemicals Used for Study ……58

Appendices Chapter 4…….59

Table B1. Other elements in raw SS, and SS-derived Biochar at Different Temperatures and Different sized Fraction…….…….59

Table B4: The fit parameters for adsorption of 10 mg/L of MB over different particles sized SS Biochar for Pseudo first-order kinetics model, Pseudo second-order kinetics model, Webber-Morris Model and Elovich Model, along with the corresponding R^2…….…….....61

Chapter 1 – Introduction

1.1 An Overview of Sewage Sludge Valorization: Biochar Production for Enhanced Adsorption of Contaminants

Water pollution is one of the significant problems worldwide and harms daily life. Industrial growth and the rise in population have resulted in a high demand for water resources, whereas enormous amounts of various wastewater are generated. The presence of pollutants such as organic matter, nutrients, pharmaceuticals, personal care products, poly- and perfluoroalkyl substances, biocides, heavy metals (for example, mercury), dyes, plastics, nanoparticles, and pathogens pose significant concerns for water quality [1]. Hence, it is critical to properly treat discharged water to minimize adverse effects on human health, aquatic species, and the ecosystem.

Dyes are colored aromatic organic compounds that absorb light and give color to the visible spectrum [2]. Most often, industries such as textiles, food, rubber, printing, cosmetics, medicine, plastic, concrete, and paper are the primary causes of dye water pollution [2]. These industries produce massive amounts of wastewater, including carcinogenic and poisonous dyes, polluting the water, and rendering it unsafe for human consumption [2].

Mercury appears in the environment in three forms: elemental, inorganic, and organic. All these forms endanger mammalian species, each having unique toxicological properties and routes within the body [3]. While natural and human processes contribute to mercury release, human activities are the primary cause of environmental mercury pollution. Notably, mercury levels in surface waters have tripled since the industrial revolution, and concentrations in Arctic marine life have risen to 10-12 times higher than in preindustrial times [4], as evidenced in Minamata disease in Japan and widespread methylmercury (MeHg) poisoning in Iraq. Global observations show alarmingly high levels of mercury in seafood consumers' blood, particularly among populations that rely on local freshwater fish from small-scale gold mining regions and those that consume marine mammals in Arctic areas [5]. Every year, approximately 316,588 to 637,233 infants in the

US exceed the US EPA's threshold of 5.8 μg/L, suggesting health hazards. Similarly, in the European Union, around 200,000 babies yearly exceed the WHO's recommended limit of 2.5 μg/g for hair mercury levels.

Sewage Sludge (SS), a byproduct of sewage disposal facilities, accumulates as urbanization accelerates, leading to significant quantities produced by wastewater treatment facilities. Handling and disposing of wastewater sludge present formidable environmental issues, as sewage sludge contains bacteria, organic contaminants, and inorganic components in various oxides and salts [6]. The United States Environmental Protection Agency classifies this sludge as a contaminant, and global regulations governing its disposal are becoming strict [7]. The Kazakh Ministry of Environment and Natural Resources reports that Kazakhstan has 180 wastewater treatment plants, 109 in industrial regions, and 71 in cities or towns [8]. In Kazakhstan, mechanical and biological treatment methods are used in most wastewater treatment facilities before tertiary treatment. Large quantities of dewatered, unstable sewage sludge are created during the treatment operations and delivered to landfills via railways. As a case, 583 million tons of wastewater were treated in 2016, resulting in 52 million tons of sewage sludge. Approximately 250–300 tons of sewage sludge with more than 70% moisture content are produced daily in Astana alone [9]. The simple disposal method of sewage sludge might eventually allow hazardous substances to enter the food chain and bioaccumulate, harming ultimately human health [10]. The most recent rules now prohibit sludge use as a natural organic fertilizer, standard NY525-2021. Therefore, thermochemical conversion, such as pyrolysis, can reduce the volume of sewage sludge, eliminate harmful compounds, and provide several added values such as bio-oil, gas, and stable pyrolytic biochar. Hence, mitigating the idea of a circular economy, this biochar could be utilized as an effective adsorbent to reduce the mercury and methylene blue concentration in water bodies (Fig. 1).

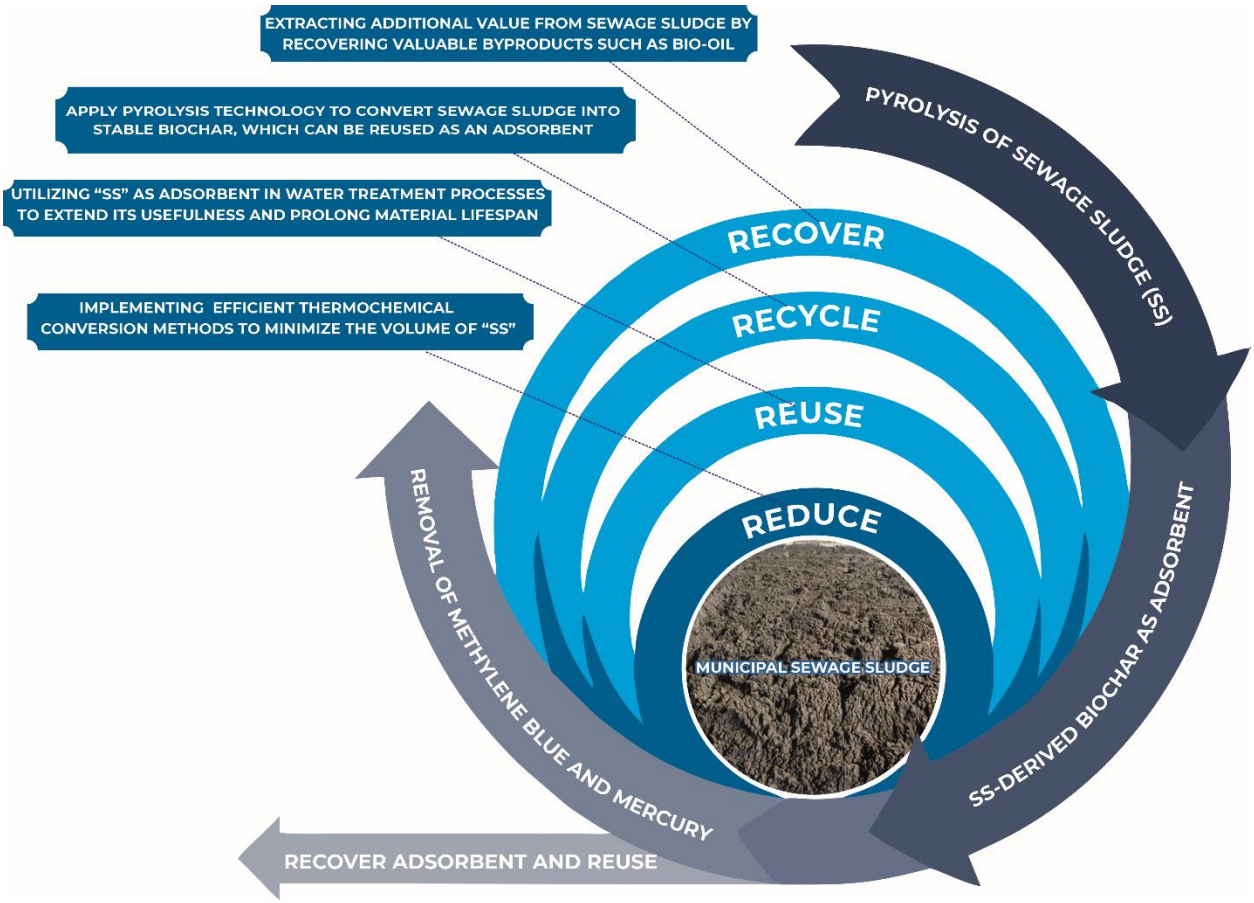

Fig.1 Integrated Circular Economy Strategy for Municipal Sewage Sludge (SS)

1.2 Aims

The thesis aimed to:

- Prepare green biochar by pyrolysis,
- Investigate the effects of pyrolysis temperature on different particle sizes of sewage sludge-derived biochar,
- Enhance the adsorption efficiency of sewage sludge-derived biochar for removing emerging contaminants from water, such as mercury and methylene blue.

1.3 Objectives

- Sample preparation using mortar and pestle to pulverize the dried sewage sludge, which

was sorted into different particle sizes using different diameters of seizes.

- Sample treatment (drying) was done on different particle sizes of sewage sludge using the carbolite furnace operating at 105 ^{o}C for 5 hrs.
- Different particle sizes of sewage sludge were pyrolyzed in horizontal fixed bed at different temperatures of 500 ^{o}C, 650 ^{o}C, and 800 ^{o}C.
- Characterization of sewage sludge-derived biochar: morphology using Scanning Electron Microscopy (SEM), elemental analysis using Inductive couple Plasma (ICP-OES), Functional group identification, Fourier Transformed infra-red spectroscopy (FTIR), and porosity using the nitrogen porosimeter.

1.4 The novelty of the research

The key novelties of the present research work are as follows:

- Assessing the impact of pyrolysis temperature on heavy metal content in various sewage sludge-derived biochar particle sizes from 800 µm-1000 µm, 400 µm- 800 µm, 100 µm-400 µm, and d ≤ 100 µm
- Exploring the mechanisms behind various particle sizes of sewage sludge-derived biochar to elucidate their effectiveness in adsorbing pollutants such as methylene blue.
- Pioneering a novel method for synthesizing NaOH-activated biochar derived from sewage sludge to treat methylene blue and mercury.

1.5 Thesis Organization

The master's thesis consists of five chapters. **Chapter 1** introduces the master thesis overview, aims and objectives, and the thesis structure.

Chapter 2 comprehensively assesses the pertinent research presented in the thesis. This section discusses thermochemical conversion technologies, sewage sludge as an adsorbent, the importance of the adsorption process over other conventional treatment methods, and the sources and global health concerns about emerging contaminants such as Methylene blue and Mercury.

Chapter 3 includes the preparation of sewage sludge, pyrolysis of sewage sludge in a horizontal quartz tube reactor, modification of sludge-derived biochar, methylene blue adsorption, and mercury adsorption. Further details on material Characterization are Fourier Transformed infrared spectroscopy (FTIR), Scanning Electron Microscopy (SEM), elemental analysis using Inductive

couple Plasma (ICP-OES), and nitrogen porosimeter.

Chapter 4 provides the research outcomes on the complete characterization of different particle sizes of the sludge-derived biochar using FTIR and ICP-OES. SEM and nitrogen porosimeter were used to characterize the sludge-derived biochar of the particle size (S_3) and its modified sewage sludge-derived biochar. The second part was the MB and mercury adsorption test.

In conclusion, the final chapter focused on examining the findings from the research detailed in this thesis and other adsorbents reported in the current literature.

Chapter 2 –Literature Review

2.1 Thermochemical Conversion

The widespread usage of petroleum-based fuels has resulted in depletion and contributed to global warming. As a result, there is a pressing need to seek alternative sustainable energy sources. Recognizing the principles of sustainable development, waste biomass has emerged as a possible solution to future energy requirements. From an economic point of view, thermochemical conversion technologies are flexible and efficient in converting biomass into valuable products, including solid fuel (biochar), liquid fuels (bio-oil or crude oil), and direct fuel Fuel (heat and power) [11]. Various thermochemical technologies include combustion, torrefaction, gasification, pyrolysis, and hydrothermal reactions. Combustion, torrefaction, gasification, and pyrolysis typically require pre-drying of feedstock with high moisture content (>20%) (Fig. 2). However, pyrolysis and hydrothermal conversion are the most successful due to their compatibility with various raw materials and high carbon production. Pyrolysis has shown promise in turning solid waste, such as sewage sludge, into bioenergy and stable biochar, thereby reducing waste volume and minimizing hazardous chemicals [12].

The general pyrolysis process follows raw sludge dried at constant weight and introduced into a furnace or reactor at a specific temperature. An inert gas (nitrogen gas) with a particular flow rate continuously passes through a pyrolysis reactor. Under a high-temperature state, the biomass is dehydrated, and several volatile organic materials and gases are released; other functional groups of organic compounds are attacked, and bonds are opened and rearranged to create new functional groups, forming carbon-rich material.

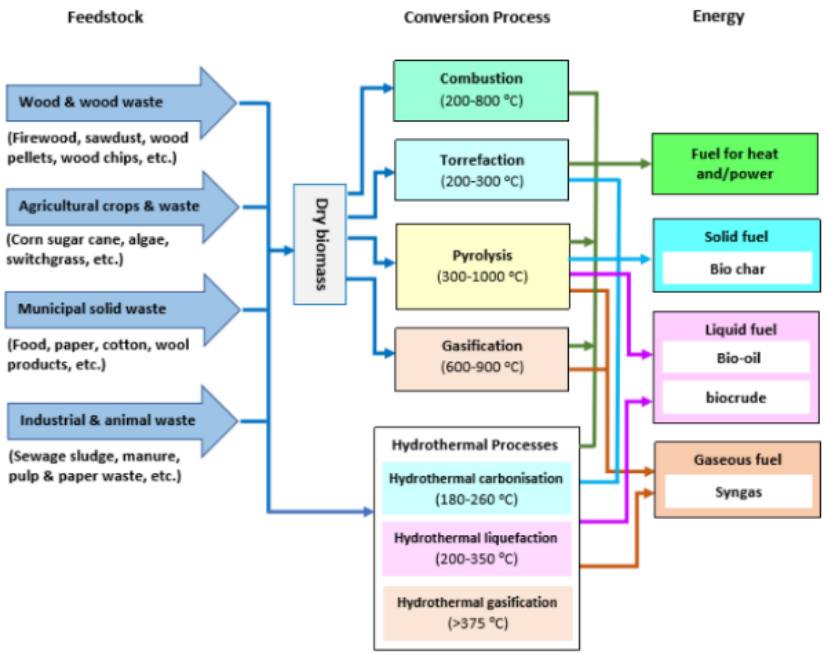

Fig. 2 Potential Biomass to Bioenergy Pathways via Thermochemical Conversion [11].

2.2 Sewage Sludge as Adsorbent

Sewage sludge (SS) is a relatively promising carbon-rich material for preparing adsorbents because of its diverse array of raw materials, complex composition, and especially numerous transition metals [13]. When sewage sludge is subjected to pyrolysis, it generates a substantial quantity of inorganic and organic materials [13]. Sludge biochar predominantly consists of elements like Silicon (Si), aluminum (Al), various forms of iron (Fe_3O_4, Fe_2O_3, FeO, and Fe_3C), as well as organic components such as hydroxyl, carboxyl, and carbonyl groups [14]. According to Yaun et al. (2013), pyrolysis temperature is an essential parameter that affects biochar's physiochemical properties and structural features, especially its carbon content [15]. Additional factors that affect the pyrolysis products include the atmosphere, particle size of biochar before pyrolysis, and heating rate. According to Taye et al. 2001 [16], sludge carbonized at 600 ◦C exhibited an increasingly porous structure with a relatively high volume of pores (0.504 mL/g) compared with those pyrolyzed at 800 ◦C and 1000 ◦C. Furthermore, Wang et al. [17] discovered that oxygen-containing functional groups increased when the pyrolysis temperature rose to 600 °C and reduced when the pyrolysis temperature increased. In terms of pyrolysis atmosphere, Huang et al. [18] discovered that sludge biochar produced under the N_2, and Ar atmospheres all showed a

robust catalytic activity toward peroxymonosulfate (PMS) for rapid removal of bisphenol A. (BPA). Also, previous studies have shown that biochar can be utilized without pre-conditioning [19] or subsequent treatment with acids, bases, or metals to improve their properties [20]. Modifying reagents, including sulfur-containing ligands [21], Fe species [22], halides [23], KOH, NaOH, and $ZnCl_2$ to enhance the sludge biochar-based material's BET area and pore volume [24] are extensively reported (Table. 1). Huang et al. [25] conducted a heterogeneous Fenton-like investigation in which the leachability of copper (Cu), iron (Fe), and zinc (Zn) from sewage sludge biochar at different pH levels was examined. According to the findings, the amounts of copper, iron, and zinc were highest at pH 3, and the concentration of metals leaching dropped as pH increased. Therefore, metal mobilization will likely occur at low pH, potentially leading to additional environmental contamination and compromising the catalyst's stability. Sewage sludge utilization research has advanced yet has overlooked the effects of pyrolysis temperature on the particle sizes of sewage sludge. Notably, leachable metallic contaminants in sewage sludge biochar pose a risk to the ecosystem [26, 27]. Jina et al., 2014, found that the leaching of metals, including Cu, Zn, and As, is higher in the larger sewage sludge particles (>0.830 mm, 0.180-0.830 mm, and 0.180 mm) [28]. Hence, a crucial gap in the literature lies in the need for more information regarding the particle size of sewage sludge before pyrolysis [29, 30]. At the same time, other studies have used sewage sludge of particle size between 1-3 mm [31] and less than 1mm before pyrolysis [32]. This discrepancy underscores the need to refine parameters in sewage sludge preparation pre- and post-pyrolysis, suggesting using smaller-sized biochar particles and maintaining a neutral pH to minimize heavy metal leaching during adsorption processes. However, adsorption characteristics under these conditions remain obscured. Hence, the study aims to (1) Prepare green biochar by slow pyrolysis, (2) Investigate the effects of pyrolysis temperature on different particle sizes of sewage sludge-derived biochar, and (3) Enhance the adsorption efficiency of sewage sludge-derived biochar for removing emerging contaminants from water, such as mercury and methylene blue.

Table 1. Comparison of different Modification of Municipal Sewage sludge and its Specific S_{BET} area

Feedstock	Modification	S_{BET} (m^2/g)	Total Pore Volume (cm^3/g)	Particle Sizes (mm)	Activation Temperature (^oC)	References
Municipal Sewage Sludge	$ZnCl_2$	18.3	0.032	0.15	550	[33]
Municipal sewage sludge	Fe/Zn, H_3PO4	41.6	0.110	0.15	450	[34]
sewage sludge	HF	50.7	0.064	nR	25	[35]
Municipal Sewage Sludge	Mixture of H_2SO_4 and $ZnCl_2$	179	0.164	0.15	550	[33]
Municipal sewage sludge	NaOH	144.27	0.25	0.2 - 0.4	650	Present work

2.3 Adsorption Process

Adsorption is a conventional technique used to eliminate pollutants in contemporary wastewater treatment alongside other methods like seawater desalination, solvent extraction, chemical oxidation, membrane separation, ion exchange, and photocatalytic degradation [36]. Despite the distinct advantages of each technology, adsorption stands out as an especially desirable option for pollutant removal. Its effectiveness, cost-efficiency, wide availability of raw materials, and the ease with which adsorbents can be modified make it a desirable option [37]. A large diversity of adsorbents is used to remove pollutants by adsorption (Table 2). However, the existing activated carbon has gradually lost its competitive advantage because of the necessity of purchase and the challenges associated with its recovery in practical application [38]. Therefore, large quantities of low-cost carbon materials, such as food waste [39], dried spent coffee [40], and sewage sludge [41], have been pyrolyzed into biochar with a large surface area and well-developed porosity to remove contaminants from water. Among them, sewage sludge biochar as an adsorbent is preferable as it contains numerous heavy metals, such as Fe^{+2} and Mn^{+2}, which act as active sites for pollutant adsorption [42].

Table 2. Adsorption Capacity of other Adsorbents in different Pollutants

Adsorbent	Adsorbate	Adsorption capacity (mg/g)	S_{BET} (m^2/g)	References
Sewage sludge	Acid brown	20.5	283	[43]
Palm oil mill sludge	Methylene blue	22.4	29.2	[44]
Sewage sludge	Methylene blue	11.78	Nil	[45]
Fe_3O_4@SiO-NH-COOH	Hg^{2+}	72.30	44.61	[46]
TiO2 NPs	Hg^{2+}	90.9	30.00	[47]
MnO_2/NaP-zeolite	Hg^{2+}	580.5	185.0	[48]

2.4 Methylene Blue (MB) Adsorption

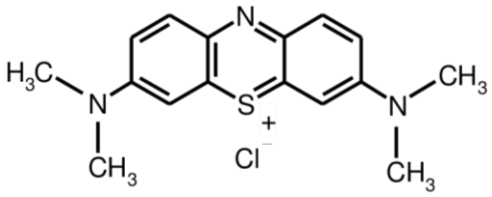

Fig. 3 Chemical nature of MB

Methylene Blue (MB) is a cationic colorant belonging to the phenothiazine family (Fig. 3). This tricyclic phenothiazine is soluble in water and some organic solvents; it has historically been used to treat malaria and methemoglobinemia, among other conditions. This molecule can penetrate the blood-brain barrier and is excreted through the urine. It was the first synthetic compound used as a clinical antiseptic [49]. It is also typically found in the effluent of the dyeing industry [2]. Dyspnoea, diarrhea, and tachycardia are just a few problems it can cause for the heart, digestive, and respiratory systems [2]. These health concerns highlight the importance of reducing the concentration of methylene blue found in natural water sources and wastewater.

2.5 Mercury Adsorption

Mercury is commonly known as a persistent atmospheric pollutant and bio-accumulative heavy metal. According to WHO, mercury is considered one of the ten chemicals to be concerned about, and the permissible limit of mercury was seen to be 0.002 mg/L [3]. According to the United Nations Environment Program (UNEP) report, around 2220 tons of mercury emissions were seen in 2015 from anthropogenic sources, which are considered globally dangerous pollutants by UNEP [50]. The anthropogenic sources include iron and steel industries [51], cement industries [52], non-ferrous metal smelting [53], chloro-alkali industry [54], and direct mercury production industries [55]. The mercury (Hg) contamination and its species are widely spread and can be detected in water resources, rocks, soil, and the air. Therefore, researchers worldwide are trying to resolve this issue and find a solution to removing Hg from water. Based on the literature, one efficient way to eliminate mercury (Hg) is by adsorption methods because of their convenience, practicality, and other separation technologies [56].

Chapter 3–Materials and Methods

3.1 Preparation of Municipal Sewage Sludge (SS)

Municipal SS treated by coagulation was obtained from a waste treatment plant in Astana (Astana Su Arnasy) during the summer (Appendices A1). The preparation of the sewage sludge was as follows (Appendices A2): Municipal sewage sludge obtained from the Astana waste treatment plant was left in a clean environment inside a fume hood for one week to dry. Further, the dried sewage sludge (SS) was pulverized and sieved into different particle sizes of 800 µm -1000 µm, 400 µm - 800 µm, 100 µm - 400 µm, and $d \leq 100$ µm, where d is the diameter of the particles. The sorted samples were then stored in air-tight glass tubes for further analysis. Before pyrolysis, the samples were further dried in a muffle furnace at 105 ºC for 5 hrs.

3.2 Pyrolysis in a Horizontal Quartz Tube Reactor

The pyrolysis experiments were carried out in a horizontal quartz tube reactor. The details of the quartz tube reactor design were first reported by [57], with the modification of parameters shown in (Fig 4). Slow pyrolysis was conducted in a horizontal fixed-bed reactor for each SS particle size. 20 g of each raw SS was weighed using the calibrated balance (Sartorius 3716MP), and the raw sludge was placed in a ceramic glass tube (with a length of 20 cm and diameter of 1.2 cm). It was then inserted in the middle of a ceramic glass tube with a length of 100 cm and an inner diameter of 5.4 cm. Pyrolysis was carried out at temperatures of 500 ºC, 650 ºC, and 800 ºC, with a heating rate of 5 ºC/min, using inert gas of nitrogen (purity of 99.5 %, 0.3 L/min, and 1 MPa). The inner temperature of the fixed bed rig was recorded using a thermocouple temperature sensor inserted into the ceramic glass tube containing the sample. After 20 mins of holding time, the pyrolysis process was stopped, and the ceramic glass tube was allowed to cool and removed later. Approximately 7-8 g of solid biochar was obtained for every 20 g raw SS sample and was denoted as S_1, S_2, S_3, and S_4 of particle sizes 800 µm -1000 µm; 400 µm- 800 µm; 100 µm - 400 µm; and $d \leq 100$ µm respectively. The biochar yield was calculated as shown below. The experiment procedure was duplicated, with the average results reported in (Fig 4). The obtained biochar was also further sieved into the four particle sizes mentioned above for further experiments.

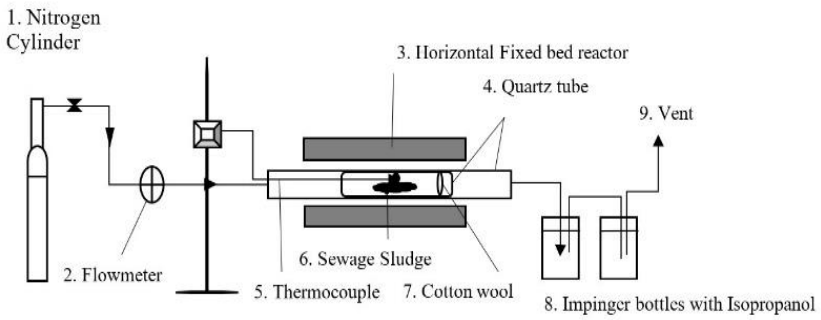

Fig. 4 Schematic Diagram of a Horizontal Quartz Tube Reactor

$$\text{Biochar Yield} = \frac{mass\ of\ char\ after\ pyrolysis\ (without\ sieving)}{mass\ of\ char\ before\ Pyrolysis} \times 100\ \% \qquad (1)$$

3.3 Modification of the Sewage Sludge-derived biochar

The samples of this work were prepared according to Poulopoulos et al. [58], with a change in reagent and pyrolysis temperature (Appendices A3). The sludge-derived biochar obtained at pyrolysis temperatures of 500 ^{o}C, 650 ^{o}C, and 800 ^{o}C of the particle size S_3 denoted as S_3-500 ^{o}C, S_3-650 ^{o}C, and S_3-800 ^{o}C were treated with NaOH at a mass ratio of 3:4 (biochar: NaOH). In the process, the biochar-NaOH mixture was poured into a crucible, covered with aluminum foil, and pyrolyzed again in a muffle furnace at temperatures of 500 ^{o}C, 650 ^{o}C, and 800 ^{o}C and a heating rate of 5 ^{o}C /min with a retention time of 20 mins. The resulting modified biochar was allowed to cool and washed with 600 ml deionized water at a constant temperature of 120 ^{o}C for 1 hour to remove the excess NaOH and reduce the alkalinity of the modified biochar. The solution was filtered, and the solid material was poured into a crucible and dried for 18 hours in a furnace at 100 ^{o}C. The NaOH-activated biochar was further sieved to maintain the particle size range noted above and was denoted as MS_3-500 ^{o}C, MS_3-650 ^{o}C, and MS_3-800 ^{o}C.

3.4 Experimental Procedure

3.4.1 Methylene Blue Adsorption: Batch adsorption tests were performed using 30 mg of SS biochar and 50 mL of methylene blue (MB) solution with a concentration ranging from 10 – 50 mg/L concentration. The solution was placed on a vibrating shaker at 150 rpm in a dark environment. A sample was withdrawn every hour, filtered through a 0.22 µm membrane, and the absorbance of the filtrate was measured using a 664 nm ultra-violet visible spectrophotometer. Before this, a calibration curve was prepared to measure MB concentration accurately (Fig 5).

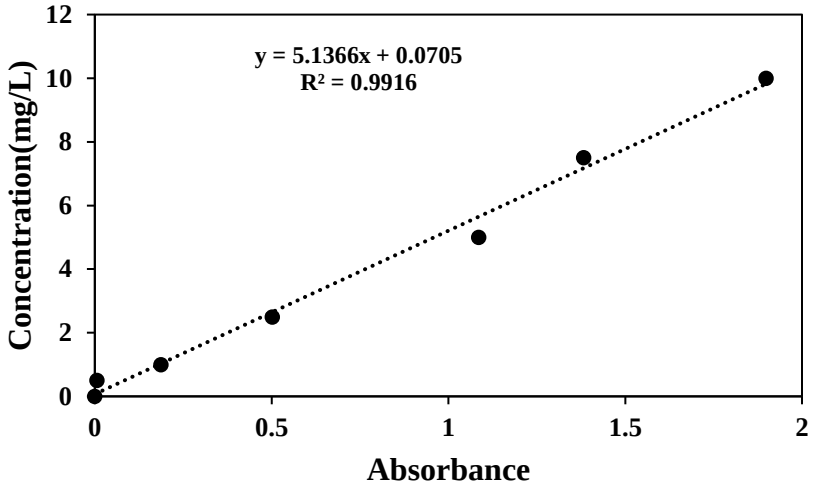

Fig 5 The Calibration Plot used for MB Quantification on UV-Vis

3.4.2 Mercury Adsorption: A 400 mg/L mercury [Hg (II)] stock solution was prepared using $Hg(NO_3)_2.H_2O$. Determinations of the total concentration of mercury in the biochar were performed based on ASTM method D6722-11[59], using an analytical complex consisting of an RA-915M atomic absorption spectrometer and a PYRO 915+ pyrolytic attachment (Lumex Ltd., St. Petersburg, Russia). Briefly, 0.5 g of the biochar was added to 50 mL mercury solutions in a polypropylene tube. The mixture was placed on a vibrating shaker (Heidolph) at a speed of 200 rpm. A 20 ml adsorbate solution was taken every 15 min, soaked onto carbon material, and inserted into the PYRO-915+ furnace to measure Hg (II) amount (Fig 6) using rapid software. Detailed operation of mercury is shown in (Appendices A4).

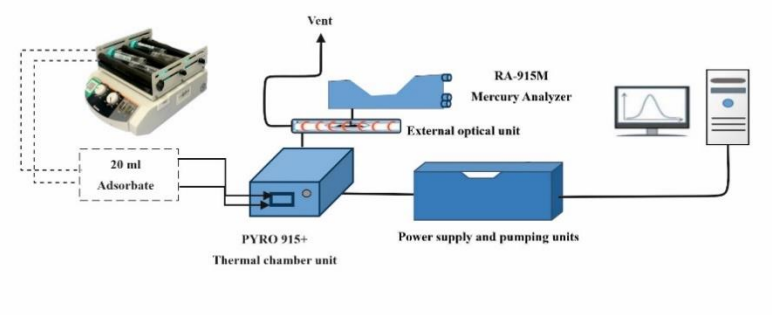

Fig. 6. Schematic Diagram of Mercury Thermal Decomposition Experimental System

All experiments were conducted at a temperature of 24 ± 2 ^{o}C and pH of 6.5. The removal efficiency (R%) and adsorption capacity (Q_e) were determined using Equation (2) and (3), respectively. The procedure was repeated twice.

$$R = \frac{C_o - C_t}{m} \times 100\ \% \qquad (2)$$

$$Q_t = \frac{(C_o - C_t)V}{m} \qquad (3)$$

Where,

Q_t: adsorption capacity as a function of time, mg/g

C_o: initial MB concentration, mg/L

C_t: final MB concentration, mg/L

V: volume of MB solution, L

m: mass of sewage sludge-derived char, g

The adsorption kinetics data were later fitted to pseudo-first order, pseudo-second order, intra-particle diffusion, and Elovich models and were used to explore the adsorption mechanisms.

Pseudo-first order kinetics: $\ln(Q_e - Q_t) = \ln Q_e - k_1 t$ (4)

Pseudo-second order kinetics: $\frac{t}{Q_t} = \frac{1}{k_2 Q_e^2} + \frac{t}{Q_e}$ (5)

Webber-Morris model: $Q_t = k_d t^{\frac{1}{2}} + C$ (6)

Elovich model: $Q_t = \left(\frac{1}{\beta}\right)\ln(\alpha_\beta) + \left(\frac{1}{\beta}\right)\ln(t)$ (7)

Where,

Q_t: adsorption amount at specific time, mg/g

Q_e: equilibrium adsorption capacity, mg/g

k_1: pseudo-first order adsorption rate constant, min^{-1}

k_2: pseudo-second order adsorption rate constant, (g/ ($\mathrm{mg.min}^{-1}$))

k_d: intraparticle diffusion rate constant, (mg/ $\mathrm{g.min}^{-0.5}$)

α: initial adsorption coefficient, ($\mathrm{mg/g.min}^{-1}$)

β: desorption coefficient, (g/mg)

t: contact time, (mins)

C: constant related to effect of the thickness of the boundary layer.

3.5 Material Characterization

The morphologies of sewage sludge, sewage sludge-derived biochar, and modified biochar were analyzed using SEM (JEOL JSM-IT200, LA). FTIR (Bruker Alpha II) was used to investigate functional groups and chemical bonds on the surface of samples with a resolution of 5 cm^{-1} and a wave number range of 400–4000 cm^{-1}. The biochar's elemental composition was determined using inductively coupled plasma (ICP) analysis (iCAPTM RQ, Thermo Fisher Scientific). The solutions for ICP were made using an ETHOS UP high-performance microwave digestion system, wherein 100 mg of sample was digested in a mixture of 3 mL of HCl, 1 mL of HNO_3, 2 ml of $HClO_4$, and 4 mL of HF at 200 °C for 1 hr, using the ETHOS UP microwave at 1800 kW, US EPA, SW-846, Method 6010C [60]. The solution was later neutralized with 10 mL of H_3BO_3 and was heated for 15 mins at 160 °C. The resulting solution was further cooled, dissolved in 30 mL deionized water, filtered using a grade of 0.22 µm, and diluted in 10X. All the reagents used were commercial grade. Pore particle size properties were recorded on nitrogen adsorption-desorption isotherm measurements at 77 K (Micromeritics 3Flex high-performance adsorption analyzer). Details of all the chemical reagents used for this study were reported in (Appendices A5).

Chapter 4 –Results and Discussion

4.1 Effects of Pyrolysis Temperature on Sewage Sludge-derived Biochar

Figure 7 shows the biochar yield for the various sludge particle sizes at different temperatures. The standard deviations upon repetitions were less than ±0.5%. The biochar mass loss was observed between 55 and 65 wt.% for all particle sizes and varied non-monotonically with the size of the particles. Figure 7 depicts a noticeable trend of a decreased biochar yield in the S_3 sample range (100 µm - 400 µm) at both 500 °C and 650 °C pyrolysis temperatures, with a heating rate of 5 °C/min. This observation aligns with the findings by Zhai et al. [61], who explored particle sizes categorized as ($d<0.25$ mm, $0.25 \text{ mm} < d < 0.83$ mm, and $d > 0.83$ mm). Their study concluded that regardless of the heating rate employed, particularly at 5 °C/min, the most significant total mass loss occurred in particle size $d<0.25$ mm at a temperature range of approximately 400 – 650 °C. This was attributed to the larger surface area of finer particles facilitating faster and more complete heat transfer. However, exceptions were noted based on our studies for powder particles (S_4: $d \leq 100$ µm), which showed a marginal increase in biochar yield at 500 °C and 650 °C and a significant reduction of biochar yield at 800 °C. In addition, Suriapparao et al. 2017 also observed lower mass loss (%) at the pyrolysis active regime (205 - 383 °C) of municipal solid waste (MSDW) of particle size 26.5 µm and higher mass loss (%) in the pyrolysis passive regime (383 - 900 °C) of 26.5µm [62]. Hence, this phenomenon could be due to more voids in large particles causing the release of primary volatiles into the gas phase without allowing them to participate in secondary decomposition reactions. However, lower voids in small particles could lead to the entrapment of the small molecules within the sample matrix, which are further released when temperature is increased, allowing secondary decomposition reactions to be possible [62]. Also, the pyrolysis temperatures at 500 °C, 650 °C, and 800 °C were found to change the particle sizes of the obtained biochar, with larger particles of sewage sludge experiencing a more significant size reduction. Hence, for any post-experiments on the adsorption studies, the biochar was further sieved and categorized according to the four sizes as used above.

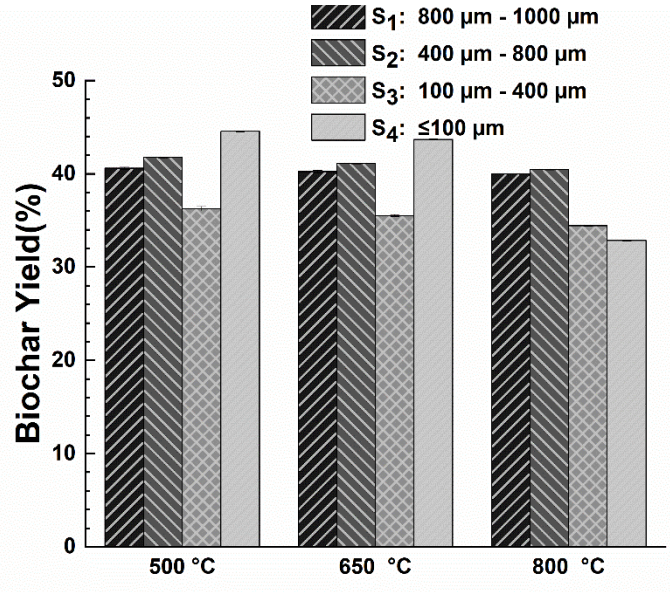

Fig 7. Effect of Different SS Particle Sizes on the Biochar Yield (%) at Different Pyrolysis Temperatures. Standard deviations were all less than ±0.5 %.

4.2 Characterization of Sewage Sludge-derived Biochar

4.2.1 Heavy Metals in SS and Sewage Sludge-derived Biochar

As mentioned above, the presence of metals such as Fe^{+2}, Zn^{+2}, and Mn^{+2} in biochar creates active sites for adsorption. Despite the significance of heavy metal content in the biochar, some leachable toxic heavy metals in sewage sludge also raise concerns regarding potential environmental impacts [26, 27]. Hence, it is essential to have a comprehensive composition of the major elements in the biochar. Figure 8 below shows the heavy metal content of Fe^{+2}, Mn^{+2}, and Zn^{+2} in the SS and the different-sized biochar obtained at different temperatures. These elements were mainly chosen because of their high metal content. Other key elements, including Ca, Mg, Na, K, Si, Ti, Pb, and Co, are shown in the (Appendices B1). The results indicate that these heavy metals were low in the raw SS but approximately doubled in the obtained biochar due to heavy metal complexation with other functional groups such as hydroxyl. These findings were similar to another study [28]. In particular, the Fe content ranged between 15 - 25 mg/g of biochar, whereas Zn and Mn ranged from 0.6-1.8 mg/g and 0.3-0.8 mg/g, respectively. Among different particle sizes, S_3 retained the highest amount of heavy metals, followed by S_1, S_4, and S_2, at pyrolysis temperatures of 500 ^oC and 650 ^oC. However, several exceptions existed at 800 ^oC, with S_4 retaining more heavy metals.

This is because as carbonization progresses, carbonaceous structures with high surface area and porosity are formed in biochar, causing the heavy metal to be immobilized in their aromatic structures, while the reduction of heavy metal is due to the breakage of the terminal C-C boundary of the biochar at high temperatures [63]. Additionally, the content of other heavy toxic metals, including Co and Pb, was in the 0.01 - 0.10 mg/g range (Appendices B1).

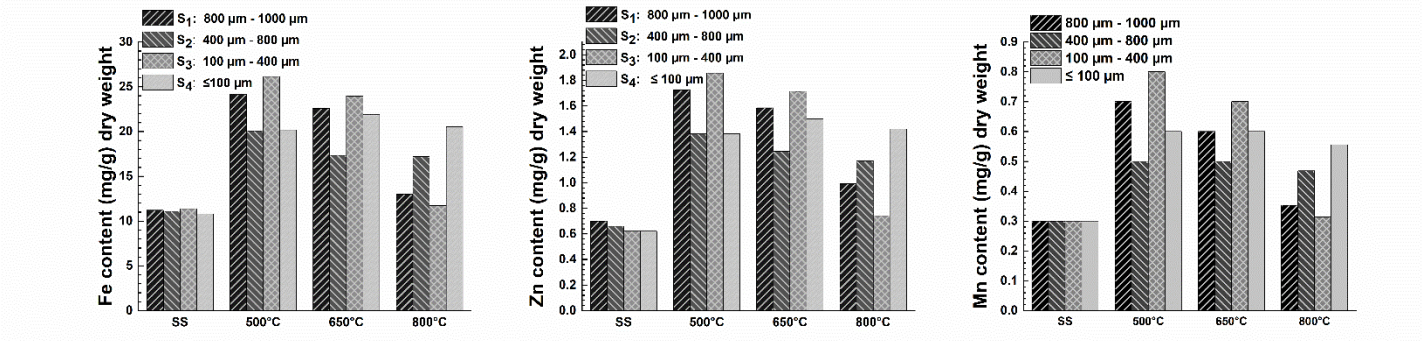

Fig. 8 Total Amount of Fe, Mn, and Zn in the Different Particle Sizes of Sewage Sludge at 500, 650, and 800 °C.

4.2.2 Surface Morphology of Sludge-derived Biochar and Modified Biochar

A crucial parameter of an adsorbent material is its surface morphology, which highlights its porous structures. Among all samples, the SEM analysis was performed only for the S_3-sized fraction of the biochar for brevity, as they showed better adsorption characteristics. Fig 9 A, B, and C show the SEM images of biochar (S_3; top), and D, E, and F show alkali-modified biochar (MS_3; bottom) surface at 500, 650, and 800 °C. The pictures highlight that fractures on the surface increased with pyrolysis temperature from 500 to 650 °C and that the hole sizes and distribution increased. However, a further increase in temperature to 800 °C resulted in a decrease in the number of surface holes, as seen in Figures 9 C and F. After modification of sewage sludge-derived biochar by NaOH, rough granular structures were observed as seen in the bottom panel of Figure 9. However, modified biochar at 800 °C also showed much less porous structures.

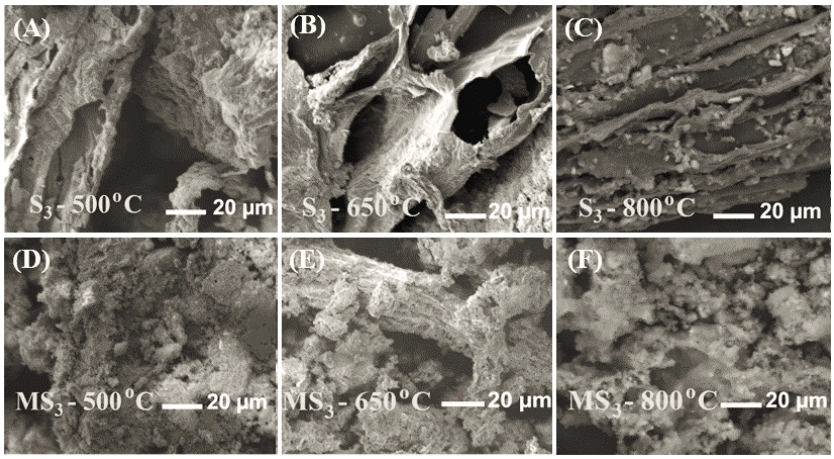

Fig. 9. Surface Morphology of Sludge-derived Biochar (S_3; A-C) and Modified Biochar (MS_3; D-F) at 500 ºC, 650 ºC, and 800 ºC.

4.2.3 Specific Surface Area of the SS-derived Biochar and modified Biochar at different temperatures

As further proof of the observation of the surface morphology, the pore characteristics of the particle size (S_3: 100 µm —400 µm) of sludge-derived biochar (S_3-500 ◦C, S_3-650 ◦C, S_3-800 ◦C) and modified biochar (MS_3-500 ◦C, MS_3-650 ◦C, MS_3-800 ◦C) at different temperatures were analyzed (Table 3).

Table 3. Specific Surface Area and Pore Characteristics for (S_3) Particle Size Biochar and Modified Biochar (MS_3) at Different Temperatures.

Sample	BET area (m^2/g)	Total pore volume (cm^3/g)	Average pore diameter (nm)
S3-500 °C	26.38	0.04	5.81
S3-650 °C	27.50	0.06	5.82
S3-800 °C	2.72	0.01	1.90
MS3-500 °C	42.30	0.14	13.54
MS3-650 °C	144.27	0.25	7.07
MS3-800 °C	27.78	0.14	1.90

The results show that the highest specific surface area was observed for MS_3-650 of 144.27 m^2/g with a total pore volume of 0.25 cm^3/g. The results also clearly suggest alkali activation to be an effective method for increasing the specific surface area of the base material [24]. For instance, even for biochar produced at 800 ^oC, which has a low BET area of 2.72 m^2/g, the alkali activation increased the BET area to 27.78 m^2/g. According to Yaun et al. 2013 [64], pyrolysis temperature is crucial in determining biochar's structural characteristics, particularly its carbon content. Their study found that the optimal temperature range for shaping sludge biochar is between 600 °C and 800 °C. Below 600 °C, incomplete carbonization of the sludge may occur, while temperatures exceeding 800 °C can lead to carbon contraction, impeding pore development by distorting the carbon structure and reducing pore volume. Zhang et al. [65] suggested that biochar pores collapse beyond a temperature of 700 ^oC, reducing the specific surface area. Likewise, Liu et al. [66] determined the surface area of the pharmaceutical sewage sludge. The results showed that biochar produced at 600 ^oC had the highest specific surface area in the temperature range of 400 – 800 ^oC.

4.2.4 Structural Characterization of SS, Sewage Sludge-derived Biochar, and Modified Biochar

The structural characterization of SS, sewage sludge-derived biochar (S_3-500 ^oC, S_3-650 ^oC, S_3-800 ^oC), and modified biochar (MS_3-500 ^oC, MS_3-650 ^oC, MS_3-800 ^oC) was further analyzed by FTIR, as depicted in Fig 10. The spectra were compared to determine the effect of pyrolysis temperature and alkali activation temperature on the presence of various functional groups. The main functional groups found in the sewage sludge, as shown in (Fig 10), includes O-H (3277 cm^{-1}), methyl (-CH2; 2917 cm^{-1}) and aliphatic group (C-H; 2849 cm^{-1}) [67], C=C group (1633 cm^{-1}) [68], N-O group (1539 cm^{-1} and 1575 cm^{-1})[69], O-H plane bending in the carboxyl group (-COOH) (1466/1418 cm^{-1}) [70], -Si-O-Si- bonds (464 cm^{-1}) [71] and Si-O group (1024 cm^{-1}) [72]. There was an appearance of peak 3345 cm-1 at a pyrolysis temperature of 500 ^oC, and it disappeared at 650 ^oC and 800 ^oC, suggesting that large hydroxyl groups were decomposed during SS pyrolysis. The aliphatic bands in the SS disappeared abruptly when heating to temperatures of 500 ^oC, 650 ^oC, and 800 ^oC, indicating organic fatty hydrocarbons were decomposed into methane, carbon dioxide, and other gases. The O-H plane bending in the carboxyl group decreased when

the temperature increased to 500 ^{o}C (1417 cm^{-1}) and 650 ^{o}C (1394 cm^{-1}) and disappeared at an elevated temperature of 800 ^{o}C. These peak bands were found in modified biochar's MS_3-500 ^{o}C, MS_3-650 ^{o}C, and MS_3-800 ^{o}C at 1411 cm^{-1}, 1410 cm-^{1}, and 1430 cm^{-1} respectively. The Si-O group in the SS decreased when the temperature increased from 500 ^{o}C (1004 cm^{-1}) to 650 ^{o}C (981 cm^{-1}) and disappeared at 800 ^{o}C. These peak bands were later found in modified biochar MS_3-500 ^{o}C, MS_3-650 ^{o}C, and MS3-800 oC at 989 cm^{-1},958 cm^{-1},945 cm^{-1}, respectively. The peak bands 871 cm^{-1} to 877 cm^{-1} were assigned to the heteroatoms of alkyl halides found in all biochar except S_3-800 ^{o}C and MS_3-650 ^{o}C. However, the appearance of peak bands 778 cm^{-1} and 776 cm^{-1} in the biochar produced at 500 ^{o}C (S_3-500 ^{o}C) and 650 ^{o}C (S_3-650 ^{o}C) were assigned to the (-CHO) carbonyl group [70] and was absent in modified biochar's. Furthermore, the peak bands at 564 cm^{-1}, 568 cm^{-1}, and 564 cm^{-1} were found in modified biochar and absent in the sewage sludge-derived biochar at 500 ^{o}C, 650 ^{o}C, and 800 ^{o}C. These peak bands were assigned to the C-N-C bend amines [70]. According to Xu et al., 2016 [71], the peak band from 448 cm^{-1} to 419 cm^{-1}, found in all biochar samples, could be attributed to -Si-O-Si-, which may act as active sites for adsorption through n- π interaction.

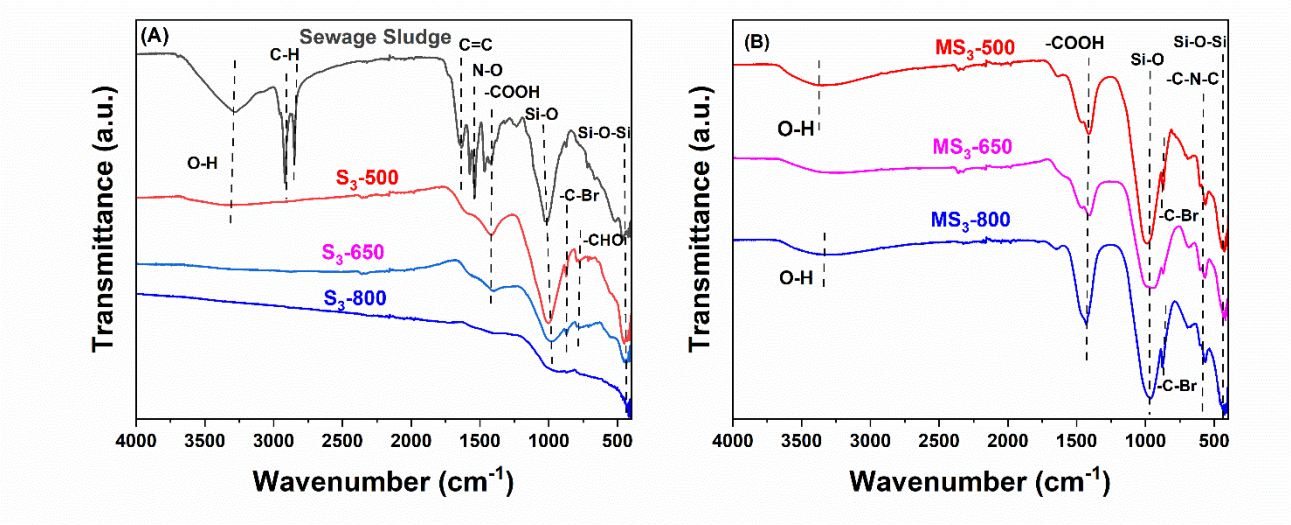

Fig. 10 Structural Characterization of Sewage Sludge, Sludge-derived Biochar (S_3), and Modified Sludge-derived Biochar (MS_3) for S_3-sized Particles at 500, 650, and 800 ^{o}C.

4.3 Batch Adsorption Studies of Methylene Blue

4.3.1 MB adsorption onto different particle sizes of Sludge-derived Biochar

From Fig.11, the particle size fraction of the sludge-derived biochar (S_1, S_2, S_3, and S_4) pyrolyzed at temperatures of 500 ◦C, 650 ◦C, and 800 ◦C were employed without pretreatment to assess their inherent behavior in an aqueous solution of methylene blue (Appendices B2). From Fig.11, the particle sizes of the sludge-derived biochar produced at a temperature of 500 ◦C showed a significant adsorption capacity with time (Fig 11A) and increased removal efficiency (Fig 11B). However, the various particle size fractions of biochar produced at pyrolysis temperatures 650 ◦C and 800 ˚C exhibited a decrease in the adsorption capacity of methylene blue at a concentration of 10 mg/L after 1 hour (Appendix B3). This was attributed to removing the O-H group at pyrolysis temperatures of 650°C and 800°C. This finding is consistent with the results reported by Khraisheh et al. (2005), who observed a decrease in the adsorption capacity of methylene blue and reactive yellow dyes due to removing O-H groups from the surface of diatomite. [71]. To reveal the exciting interplay of each particle size of the sludge-derived biochar and MB adsorption process from a solution of 10 mg/L – 50 mg/L, the study used individual particle size fractions produced at a temperature of 500 ˚C as the basis of the study with a constant adsorbent mass of 30 mg, depicted in Figure 12.

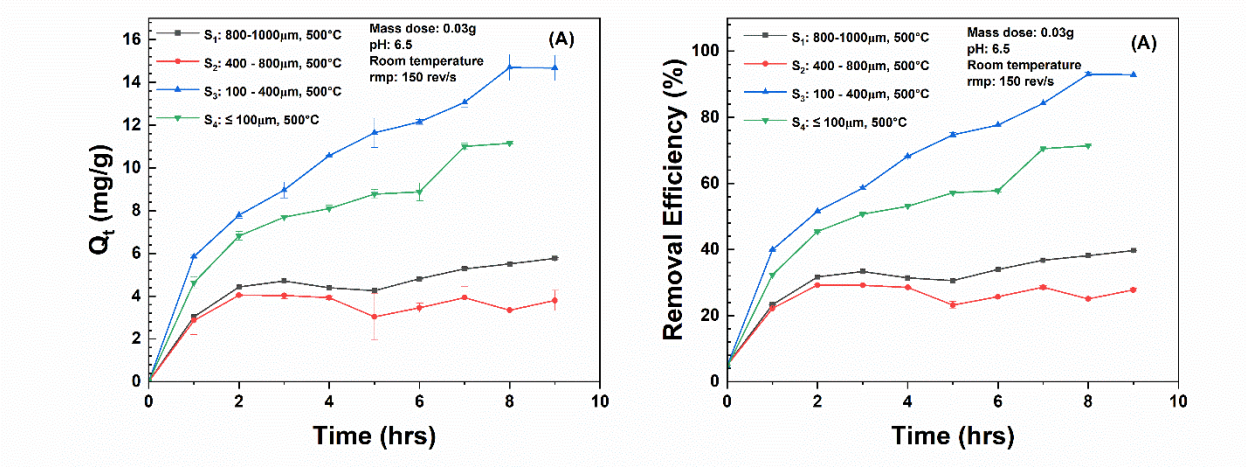

Fig 11. MB Adsorption Capacity versus Time (10 ppm MB, Adsorbent mass: 30 mg, pH of 6.5 at 25 °C, oscillating speed at 150 rpm).

4.3.2 Effect of Methylene Blue Concentration on Adsorbent Mass

From Fig. 12, the adsorption process of methylene blue onto the different-sized fractions (S_1, S_2, S_3, and S_4) produced at 500 ◦C showed an increased adsorption capacity and a decreased removal efficiency as the initial MB concentration increased from 10 mg/L to 50 mg/L using a constant adsorbent mass of 30 mg. This phenomenon could be due to the adsorbent's unavailable active sites and the repulsive interactions between the methylene blue molecules as the MB concentration increases [73]. However, particle size (S_3: 100 µm - 400 µm) showed a remarkable equilibrium adsorption capacity of 22 mg/g in 50 mg/L MB solution of 50 mL, compared to S_1: 800 - 1000 µm (16 mg/g), S_2: 400 - 800 µm (14.5 mg/g), and S_4: ≤ 100 µm (17 mg/g). The impressive performance of S_3: 100 - 400 µm was possibly due to more active sites (heavy metal-rich) based on the inductively coupled plasma results. Hence, to understand the underlying key mechanism of each particle size produced at 500 ◦C (S_1-500, S_2-500, S_3-500, S_4-500) from a solution of 10 mg/L of MB, the experimental data was fitted to adsorption kinetics models.

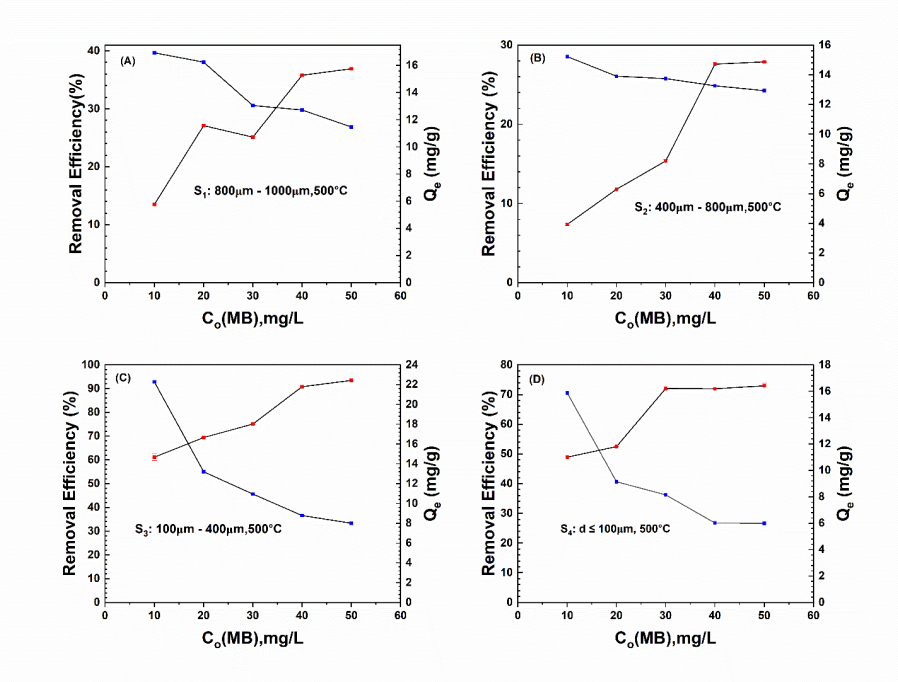

Fig 12. Adsorption Capacity versus Initial MB Concentration (10 ppm MB, Adsorbent mass: 30 mg, pH of 6.5 at 25 °C, oscillating speed at 150 rpm).

4.3.3 MB Adsorption Kinetics of Different Particle Sizes of Sewage Sludge-Derived Biochar

The Webber Moris, Elovich Model, Pseudo-first , and Pseudo second-order kinetic models were used to study MB adsorption onto different particle sizes of sludge-derived biochar (Appendices B4).

4.3.3.1 Pseudo first-order and Pseudo second-order Model

From Fig 13, it was observed that the Pseudo second-order (B) completely captured the adsorption process due to the strong correlation coefficient obtained for the biochars produced at 500 °C of particle size fractions (S_1: 800 µm -1000 µm, S_2: 400 µm - 800 µm, S_3: 100 µm - 400 µm, and S_4: d ≤ 100 µm). The calculated Qe values of S_1 (5.6mg/g), S_2 (3.7mg/g), S_3 (17 mg/g), and S_4 (12 mg/g) obtained from the Pseudo second-order model were more accurate compared to the experimental values of S_1 (5.7mg/g), S_2 (3.7mg/g), S_3 (15 mg/g) and S_4 (11mg/g). The pseudo-second-order had an error percentage of less than 11%. In comparison, the pseudo-first-order had an error percentage of less than 13 % (Eq. 7). The adsorption process is predicted to be governed by chemisorption or physisorption by statistically fitting kinetic data to a specific model [74]. In theory, fitting pseudo-first and pseudo-second kinetic data cannot definitively determine if a system is experiencing chemisorption.[75]. To better understand the phenomenon, the Webber-Morris method was used to predict the role of diffusion in the adsorption of methylene blue, as shown in Figure 14.

$$|\text{Error Percentage}| = \frac{\text{Experimental } Q_e - \text{Calculated } Q_e}{\text{Experimental } Q_e} x\ 100 \qquad (7)$$

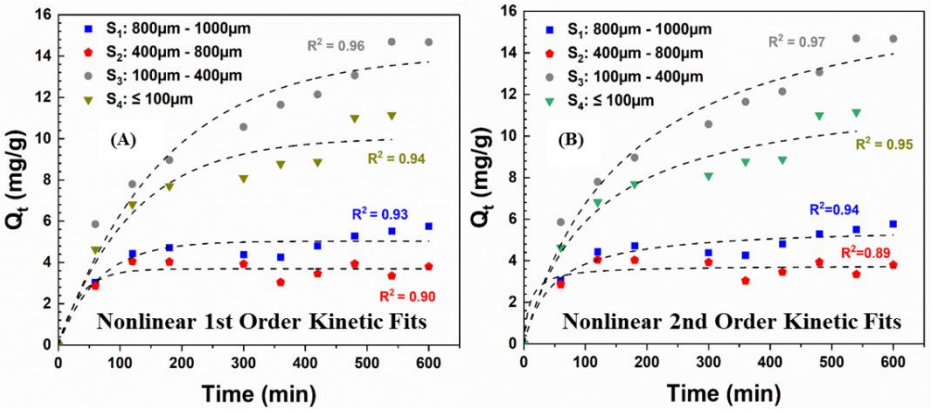

Fig.13 Nonlinear 1st Order(A) and 2nd order(B) Kinetic Fit for MB Adsorption onto Sludge-derived Biochar of Different Particle Sizes: (Adsorbent mass: 30 mg, C_o:10 mg/g, pH: 6.5)

4.3.3.2 Webber Moris Model

According to the Webber-Morris model [76], intra-particle diffusion strongly controls the system if the adsorption capacity qt is linearly connected with the square root of time that passes through the origin (Fig. 14). Based on the graph, it was observed that no particle size of the sludge derived biochar passed through the origin. However, it had good R^2 values between 0.83 and 0.98 (except for S_2)(Appendices B4). The intraparticle diffusion (K_d) rate of the sludge-derived biochar produced at 500 °C for sized fraction S_3: 100 µm - 400 µm had a higher K_d value of 0.58 compared to S_1: 800 µm -1000 µm (0.19), S_2: 400 µm - 800 µm (0.1), and S_4 (0.44) suggesting a greater mass transfer resistance to intraparticle diffusion and potentially longer times to reach equilibrium. The lower constant value (C) 0.8 of the sewage sludge biochar (S_3: 100 µm - 400 µm) suggests a thicker boundary layer. Also, the higher correlation value of 0.99 of the particle size fraction S_3: 100 µm - 400 µm compared to S_1: 800 µm -1000 µm (0.83), S_2: 400 µm - 800 µm (0.5), and S_4 (0.95) indicates that the model provided an adequate description of the experimental data. Despite the complexities of the pore structures of particle size fraction (S_3: 100 µm - 400 µm), the model can still capture the underlying adsorption kinetics reasonably well. Hence, intra-particle diffusion processes were not the primary controlling step during adsorption, whereas liquid film diffusion may also be a crucial factor, as noted earlier in the literature [77].

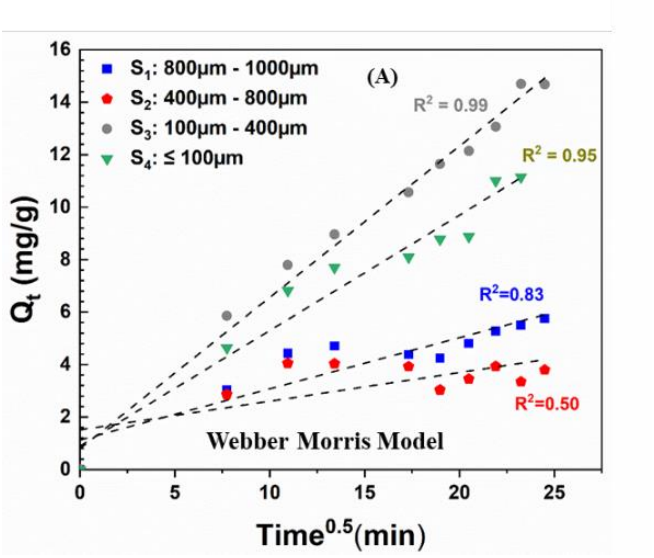

Fig.14 Intra-particle Diffusion of MB Adsorption on Sludge-derived Biochar of Different Particle sizes (C_o:10 mg/g, pH: 6.5)

4.3.3.3 Elovich Model

Furthermore, the Elovich plot's (Fig 15) strong fit to the kinetic data and the high correlation coefficient values obtained suggest that MB adsorption on particle size fractions (S_1: 800 µm - 1000 µm, S_2: 400 µm - 800 µm, S_3: 100 µm - 400 µm, and S_4: d ≤ 100 µm) of sewage sludge biochar is not a straightforward first or second-order reaction but a complex process [78]. Additionally, the model fit parameters (Appendices B4) α and β reveal comparable initial adsorption and desorption rates of 0.17 and 0.22 for S_3, indicating better adsorption characteristics.

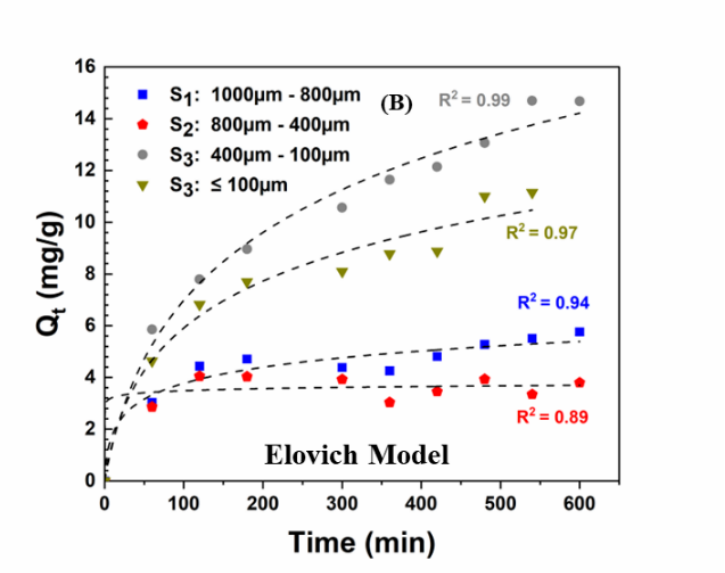

Fig.15 Elovich Model of MB Adsorption on Sludge-derived Biochar of Different Particle Sizes (C_o:10 mg/g, pH: 6.5)

4.4 Effect of Adsorbent (S_3:100 – 400 µm) Dosage in MB Solution

The effect of adsorbent (S_3:100 – 400 µm) dosage was studied using 10 mg/L of methylene blue and varied adsorbent masses of 10 mg, 30 mg, 50 mg, and 100 mg. From Fig. 16A, it was observed that the adsorption capacity of methylene blue onto the sewage sludge-derived biochar increases with increasing time. After 4 hours, the sewage sludge-derived biochar showed decreased adsorption capacity for an adsorbent mass of 10 mg. From Fig. 16B, the results suggest that 30 mg is the minimum mass required to remove methylene blue from aqueous water effectively. However, increasing the adsorbent mass from 30 mg to 100 mg slightly increased the removal efficiency from 92% to 95% (Fig. 16C).

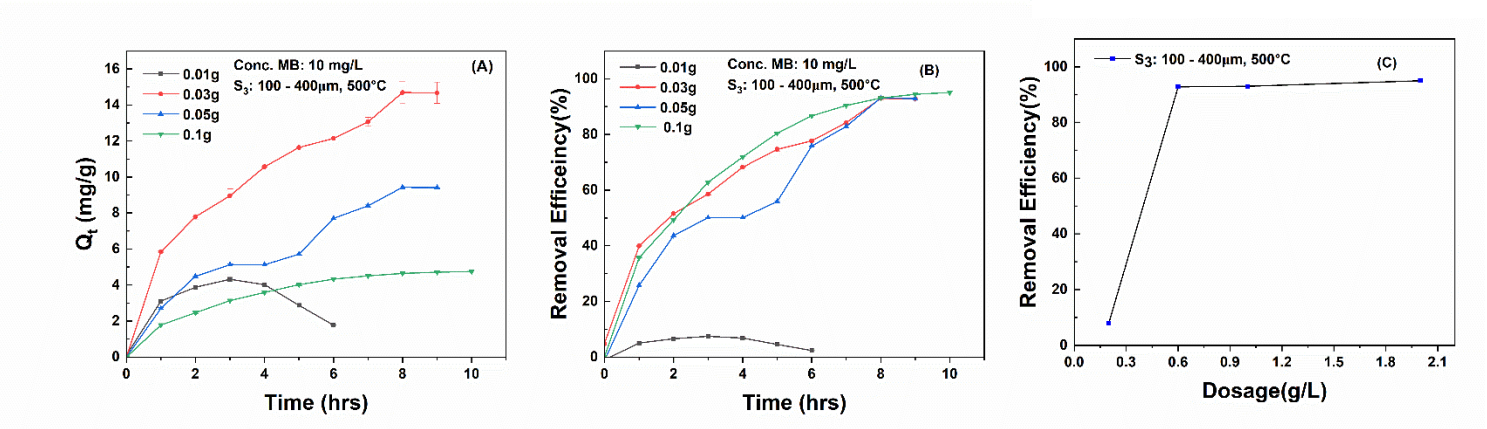

Fig. 16 Effect of Adsorbent Dosage (Co = 10 mg/g, pH =6.5)

4.5 Influence of pyrolysis temperature and alkali activation on adsorption

4.5.1 Methylene Blue Removal

Further, the study examined the effect of pyrolysis temperatures of 500, 650, and 800 ◦C and Akali activation on the adsorption of particle size fraction (S_3) for removing 400 mg/L of methylene blue from an aqueous solution with an adsorbent mass of 500 mg. Samples were taken every 15 minutes at an agitation speed of 200 rev/min and followed the same experimental procedure above for methylene blue removal studies. Fig. 17 shows a time-dependent rise in the adsorption capacity of methylene blue (A) and an increase in removal efficiency (B). MS_3-650 ◦C had the highest

adsorption capacity in methylene blue at 35 mg/g, possibly due to its higher surface area of 144.27 m^2/g. Despite MS_3-800 ◦C having a surface area of 27.78 m^2/g compared to S_3-500 ◦C of 26.38 m^2/g, the adsorption capacity of methylene blue onto S_3-500 ◦C (21 mg/g) was higher than MS_3-650 ◦C (19 mg/g), and this was attributed to the larger pore diameter of 5.81 nm of S_3-500 ◦C as compared to 1.90 nm of MS_3-800 ◦C, which means that the average pore diameter of the biochar influenced the quantity of methylene blue molecules to be adsorbed. Moreover, removing the O-H group from the surface of the biochar at temperatures of 650 ◦C and 800 ◦C led to a decrease in methylene blue adsorption capacity [72]. These results suggest that the surface functional group, the surface area, and the average pore diameter influenced methylene blue adsorption.

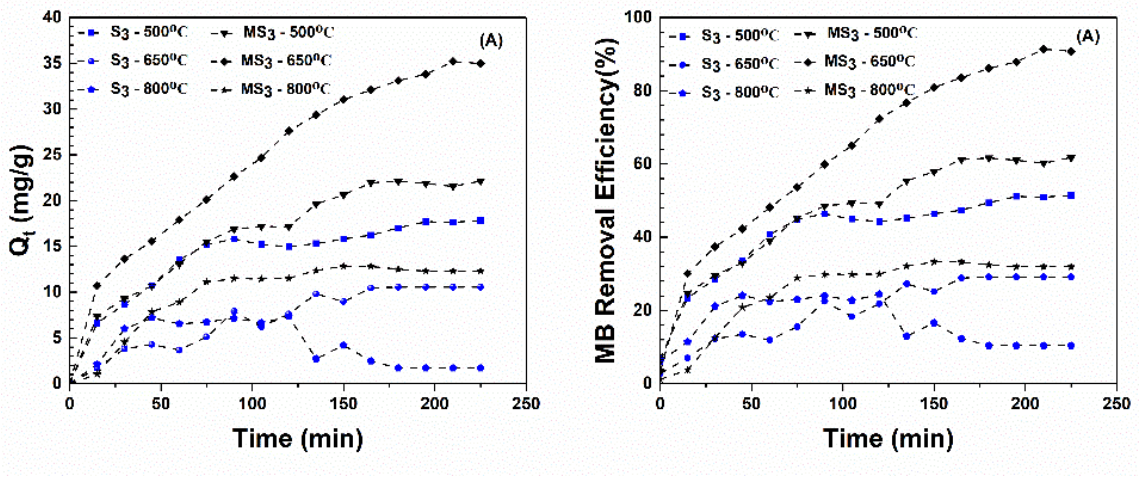

Fig 17. Methylene blue Adsorption with Time (C_0: 400 mg/L, room temp, pH:6.5, agitation speed; 200 rev/min)

4.5.2 Mercury Removal

Figure 18 shows a time-dependent rise in mercury removal efficiency(B) and adsorption capacity(A) with modified biochars (MS_3-500 ◦C, MS_3-650 ◦C, MS_3-800 ◦C), demonstrating a remarkable increase in adsorption capacity compared to the sewage sludge-derived biochars (S_3-500 ◦C, S_3-650 ◦C, S_3-800 ◦C). The higher surface area of MS_3-650 ◦C facilitated more significant interaction with mercury ions. MS_3-650 ◦C may have had an optimum pore diameter, enabling efficient mercury ion adsorption with a significant adsorption capacity of 36 mg/g and a 93%

removal efficiency, surpassing the other samples (MS_3-500 C: 84%, MS_3-800 C: 61%, S_3-500 C: 58%, S_3-650 C: 53%, S_3-800 C: 35%). These results suggest that surface area was the dominant factor influencing mercury adsorption.

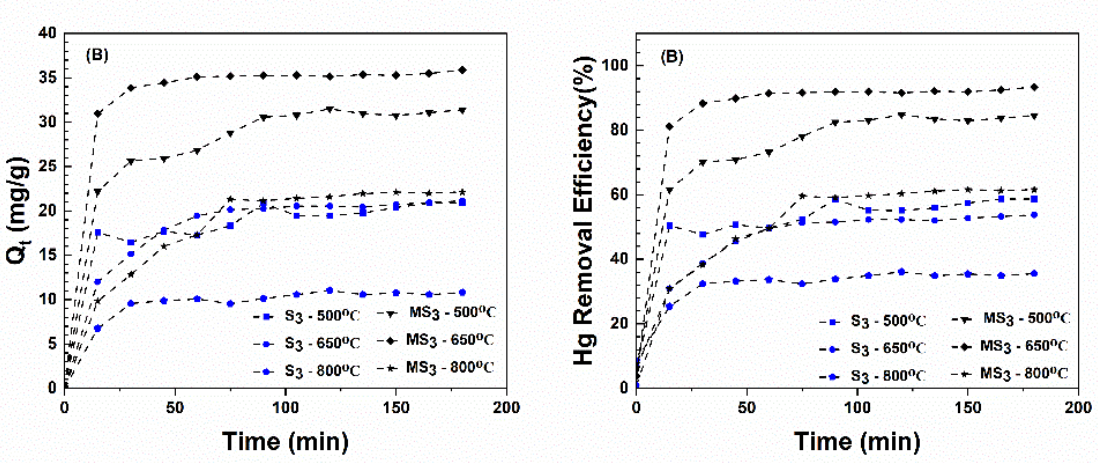

Fig 18. Mercury Adsorption with Time (C_0: 400 mg/L, room temp, pH: 6.5, agitation speed: 200 rev/min)

4.6 Possible Mechanism of MB and Hg^{+2} Adsorption onto Sludge-derived Biochar and Modified Biochar

According to the FTIR and ICP results, nitrogen functional groups, O-H group, and -Si-O-Si- and cations such as (Ca^{+2}, Mg^{+2}, Na^{+}, and K^{+}) may participate in methylene blue and mercury adsorption onto sewage sludge-derived biochar (S_3) and modified biochar (MS_3). The -Si-O-Si- group mainly acts as an active site for dye adsorption through n-π interactions [71]. Mitrogiannis et al. (2015) demonstrated that the liberation of Ca^{+2} and Na^{+} cations from the biochar surface into the solution after MB adsorption validated the involvement of the cation exchange mechanism.[79]. According to Lu et al., 2015, an alkaline biochar surface contains oxygen-containing functional groups and inorganic material components [80]. Also, Leng et al., 2015, reported that MB adsorption onto the biochar surface is through electrostatic bonding [81]. Additionally, Shi et al. 2014 [82] found that sludge biochar and MB adsorption mechanisms involve electrostatic interactions, ion exchange, and surface complexation. Based on observations of Takaya et al., 2016, the surface area is a key factor influencing heavy metal ions adsorption, contributing to further reaction[83], while Wang et al.,2022 suggested that Hg (II) ions are

adsorbed onto sludge biochar through ion exchange interactions[84]. Despite this, mercury can interact with the hydroxyl group by electrostatic interactions [85]. In summary, Figure 18 depicts the potential mechanisms involved in the adsorption of MB and Hg^{+2}. These mechanisms encompass electrostatic interactions, ion exchange, hydrogen bonding, and other interactions.

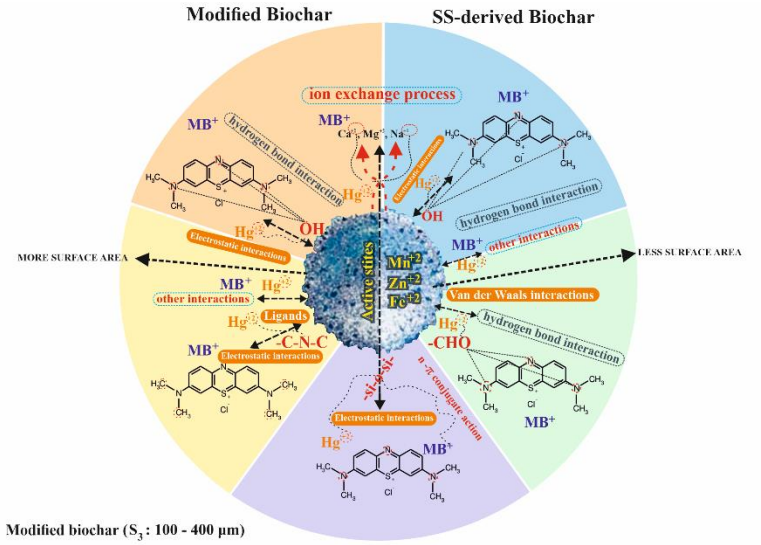

Fig 19. Possible interactions of Methylene Blue (MB) and Mercury (Hg^{+2}) Adsorption onto Biochar Derived from Sludge and Modified Biochar

4.7 Comparative study with other adsorbent materials

A comparative study was based on MB dye and mercury adsorption capacity from an aqueous solution onto several adsorbents [86-92] and included novel modified biochar denoted as MS3-650 ºC (Fig 20). Fig 20 shows the adsorption capacity results of Hoselett et al., 2020 (mixed municipal discarded material) [86], chitosan nanocomposite [87], kaolin [88], Hickory chips char [89], activated carbon [90], C. arietinum waste [91], Corn straw [92]. Remarkably, pyrolysis of municipal sewage sludge waste at 650 ºC, coupled with NaOH activation at the same temperature, emerged as a standout candidate. Through meticulous preparation, MS_3-650 ºC experienced significant physical and chemical transformations, resulting in a cost-effective material with a high affinity for pollutants such as methylene blue and mercury. This biochar exhibits auspicious potential for future environmental endeavors. MS_3-650 ºC utilization not only tackles pollution

issues but also adheres to the principles of a circular economy. By repurposing waste materials, MS_3-650 ºC demonstrates sustainability and resource optimization, leading to a more robust and ecologically responsible future.

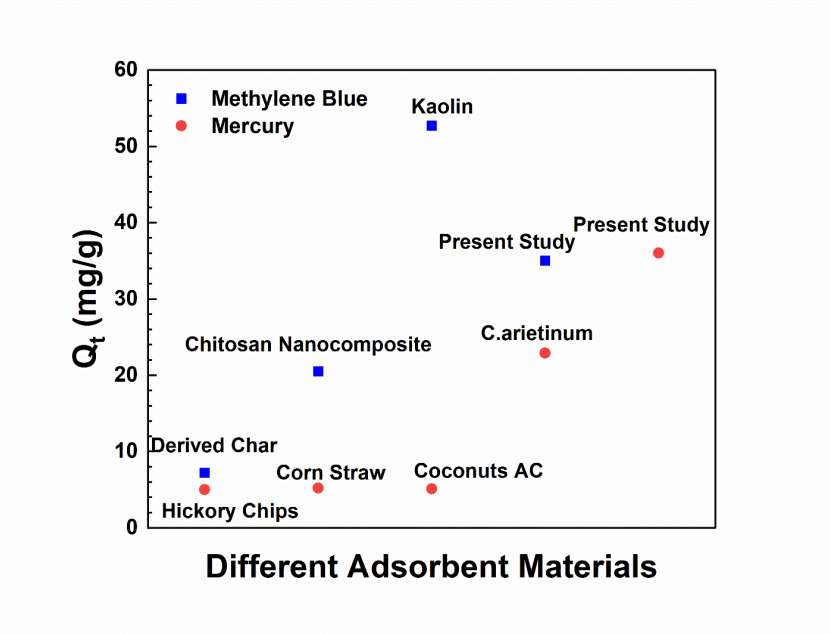

Fig 20. Comparison of Adsorption Capacity with Other Adsorbents Materials

Chapter 5 – Conclusion

In conclusion, the study of this work revealed that the preparation condition of sewage sludge, such as particle sizes before pyrolysis, is critical to enhancing the heavy metal content in the sewage sludge-derived biochar. In addition, a higher pyrolysis temperature of 800 ºC increases the mass loss of sewage sludge-derived biochar. Notably, smaller particle sizes of the sludge-derived biochar (S_3: 100 - 400 µm) and (S_4: d ≤ 100 µm) exhibited enhanced heavy metal retention such as Fe^{2+}, Mn^{2+}, Zn^{2+}, and Ti^{2+}, suggesting potential benefits adsorbent for wastewater treatment and remediation. This study also demonstrated that sewage sludge-derived biochar with different particle sizes behave differently across mediums such as methylene blue and mercury solution. Hence, particle sizes in the 100 – 400 µm range and d ≤ 100 µm tend to have a stable adsorption capacity in methylene blue compared to larger sewage sludge particles. The study identified the particle size 100 – 400 µm as the best adsorbent due to the high adsorption capacity and strong correlation values. Furthermore, the surface modification technique demonstrated promise in enhancing sewage sludge derived-biochar's adsorption capacity with the highest adsorption capacity of 35 mg/g (MS_3-650 ºC) of methylene blue and 36 mg/g (MS_3-650 ºC) of mercury. Therefore, pyrolyzing sewage sludge at a temperature of 650 ºC and activating it with NaOH at the same temperature is a promising methylene blue and mercury removal strategy.

Future research endeavors could explore the modified biochar (MS_3-650 ºC) mechanisms towards methylene blue and mercury adsorption and its long-term stability and effectiveness in real-world wastewater treatment scenarios, providing valuable insights for practical applications.

Future research could also explore alternative treatment methods by optimizing process parameters such as pyrolysis flow rate and heating rate and investigating their impact on the heavy metal content of the sewage sludge-derived biochar particle sizes and oil yield.

Future research could include adsorption isotherms to provide more information on the biochar behavior in pollutant adsorption.

Finally, the pyrolysis of SS must be prepared carefully to minimize the contamination of biochar from the produced oil; hence, it is recommended to be treated with acids, bases, or other modifying agents for better adsorption of pollutants.

References

[1].M. C. Villarín, S. Merel, “Paradigm shifts and current challenges in wastewater management,” Journal of Hazardous Materials, Vol. 390, 15 May 2020, 122139

[2]. M.I. Din, R. Khalid, J. Najeeb, Z. Hussain, "Fundamentals and photocatalysis of methylene blue dye using various nanocatalytic assemblies- a critical review," J Clean Prod, vol.298, pp. 126567, 2021.

[3] Who, 2016. The Public Health Impact of Chemicals: Knowns and Unknowns. World Health Organization.

[4]. C. H. Lamborg, C. R. Hammerschmidt, K. L. Bowman, G. J. Swarr, K. M. Munson, D. C. Ohnemus, P. J. Lam, L.E. Heimbürger, M. J. A. Rijkenberg & M. A. Saito, “A global ocean inventory of anthropogenic mercury based on water column measurements,” Nature volume 512, pages65–68 (2014)

[5]. D. V. Sheehan, J. M. Giddens, and I. S. Sheehan,” Status Update on the Sheehan-Suicidality Tracking Scale (S-STS),” Clinical Neuroscience, 11(9-10): 93–140, 2014.

[6]. Z.L. Du, A.B.Hu., Q.D. Wang, Ai, J., W.J. Zhang, Y. Liang., M.X. Cao, H. J.Wu., D.S., Wang., "Molecular composition and biotoxicity effects of dissolved organic matters in sludge-based carbon: effects of pyrolysis temperature," J. Hazard. Mater. Vol. 424, pp. 12734, 2022.

[7]. J. Ai., W. Zhang., G. Liao., F. Chen., D. Wang., "A novel waste activated sludge multistage utilization strategy for preparing carbon-based Fenton-like catalyst: catalytic performance assessment and micro-interfacial mechanisms, Water Res., vol. 150, pp. 473-487, 2019. DOI: 10.1016/j.watres.2018.11.085

[8]. T. Ozturk, H. Altinsoy, M. Türkeş & M. L. Kurnaz., "Simulation of temperature and precipitation climatology for the Central Asia CORDEX domain using RegCM 4.0," Climate Research, vol. 52, pp. 63-76, 2012.

[9]. V. N. Pavlova., S. E. Varcheva., R. Bokusheva & P. Calanca "Modelling the effects of climate variability on spring wheat productivity in the steppe zone of Russia and Kazakhstan," Ecological Modelling, vol. 277, pp. 57-67, 2014.

[10]. S.J. Yuan., X.H. Dai, "Sewage sludge-based functional nanomaterials: development and applications," Environ. Sci. Nano, vol. 4, pp. 17–26, 2017.

[11]. E. D. Boateng., & O.W. Achaw., “Bioenergy and biofuel production from biomass using thermochemical conversions technologies—a review,” AIMS Energy, Vol.10(4),pp.585–647, 2022

[12]. M. Hu., Z. Ye., H. Zhang., B. Chen., Z. Pan., & J. Wang., "Thermochemical conversion of sewage sludge for energy and resource recovery: technical challenges and prospects," Environ. Pollut. and Bioavailability, Vol. 3(1), pp.145-16, 2021.

[13]. S. Li, D. Huang, M. Cheng, Z. Wei, L. Du, G. Wang, S. Chen., L. Lei., Y. Chen., R. Li., "Application of sludge char nanomaterials in Fenton-like processes: Degradation of organic pollutants, sediment remediation, sludge dewatering," Chemosphere, vol. 307, pp. 135873, 2022.

[14]. Gao, N., Quan, C., Liu, B., Li, Z., Wu, C., Li, A., 2017. Continuous pyrolysis of sewage sludge in a screw-feeding reactor: products characterization and ecological risk assessment of heavy metals. Energy Fuels 31, 5063–5072.

[15]. Yuan, Y., Yuan, T., Wang, D., Tang, J., Zhou, S., 2013, sewage sludge biochar as an efficient catalyst for oxygen reduction in a microbial fuel cell.Bioresour.Technol.144,115-120

[16]. Tay, J.H., Chen, X.G., Jeyaseelan, S., Graham, N., 2001. Optimizing the preparation of activated carbon from digested sewage sludge and coconut husk. Chemosphere 44, 45–51.

[17]. X.P. Wang., L. Gu., P. Zhou., N.W. Zhu., CX Li., H. Tao., H.F. Wen., D.F. Zhang, "Pyrolytic temperature-dependent conversion of sewage sludge to carbon catalyst and their Performance in persulfate degradation of 2-Naphthol," Chem. Eng. J, vol. 324, pp. 203–215, 2017.

[18]. B.C. Huang., J. Jiang., G.X. Huang., H.Q. Yu., "Sludge char-based catalysts for improved pollutant degradation by activating peroxymonosulfate," J. Mater. Chem, vol. 6, pp. 8978–8985, 2018.

[19]. Liu, J., Jiang, S., Chen, D., Dai, G., Wei, D., Shu, Y., 2020, "Activation of persulfate with char for degradation of bisphenol A in soil, J. Chem. Eng., Vol. 381, pp. 122637, 2020.

[20]. Lei, Y., Guo, X., Jiang, M., Sun, W., He, H., Chen, Y., Thummavichai, K., Ola, O., Zhu, Y., Wang, N., "Co-ZIF reinforced cow manure char (CMB) as an effective peroxymonosulfate activator for degradation of carbamazepine, Applied catalysis B: Environmental, Vol. 319, pp. 121932, 2022.

[21]. Park, J.H., Wang, J.J., Zhou, B., Mikhael, J.E.R., DeLaune, R.D., "Removing mercury from aqueous solution using sulfurized char and associated mechanisms, Environ. Pollut., Vol. 244, pp. 627-635, 2019.

[22]. Wang, H., Liu, Y., Ifthikar, J., Shi, L., khan, A., Chen, Z., Chen, Z., "Towards a better understanding on mercury adsorption by magnetic bio-adsorbents with gamma-Fe2O3 from pinewood sawdust derived hydrochar: influence of atmosphere in heat treatment, Bioresour. Technol, Vol. 256, pp. 269 -276, 2018a.

[23]. Wang, T., Liu, J., Zhang, Y., Zhang, H., Chen, W., Norris, P., Pan, W., "Use of a non-thermal plasma technique to increase the number of chlorine active sites on char for improved mercury

removal," J. Chem. Eng., Vol.331, pp. 536-544, 2018b.

[24]. M.M. Mian., G. Liu., B. Fu., "Conversion of sewage sludge into environmental catalyst and microbial fuel cell electrode material: A review," Sci. Total Environ, vol. 666, pp. 525–539, 2019.

[25]. Y.F. Huang., Y.Y. Huang., P.T. Chiueh., S.L. Lo., "Heterogeneous Fenton oxidation of trichloroethylene catalyzed by sewage sludge char: Experimental study and life cycle assessment," Chemosphere, vol. 249, pp. 126139, 2020.

[26]. J. Ren, J. Cao, X. Zhao, Y. Liu, "Fundamentals and applications of char in biomass tar reforming," Fuel Process Technol, vol. 216, pp. 106782, 2021.

[27]. X. Wang, C. Li, Z. Li, G. Yu, Y. Wang, "Effect of pyrolysis temperature on characteristics, chemical speciation and risk evaluation of heavy metals in char derived from textile dyeing sludge," Ecotox Environ Safe, vol. 168, pp. 45-52, 2019.

[28]. H. Jina., R. O. Arazo., J. Gaoe., S. Capareda., Z. Changa, "Leaching of heavy metals from fast pyrolysis residues produced from different particle sizes of sewage sludge," Journal of Analytical and Applied Pyrolysis, vol. 109, pp. 168–175, 2014.

[29]. A. Ahmad., N. Khan., B. S. Giri., P. Chowdhary., P. Chaturvedi. "Removal of methylene blue dye using rice husk, cow dung, and sludge char: Characterization, application, and kinetic studies," Bioresource Technology, vol. 306, pp. 12320, 2020.

[30]. Zeng, H.; Qi, W.; Zhai, L.; Wang, F.; Zhang, J.; Li, D. Preparation and Characterization of Sludge-Based Magnetic Char by Pyrolysis for Methylene Blue Removal. Nanomaterials 2021, 11, 2473. https:// doi.org/10.3390/nano111024.

[31]. Y.H. Lia., F.M. Chang., B. Huang., Y.P. Song., H.Y. Zhao., K.J. Wang." Activated carbon preparation from pyrolysis char of sewage sludge and its adsorption performance for organic

compounds in sewage," Fuel, vol. 266, pp. 117053, 2020.

[32]. M. Hu., W. Deng., M. Hu., G. Chen., P. Zhou., Y. Zhou., Y. Su., "Preparation of binder-less activated char briquettes from pyrolysis of sewage sludge for liquid-phase adsorption of methylene blue," Journal of Environmental Management, vol. 299, pp. 113601, 2021.

[33]. Y.X. Huang, Y.R. Sun, Z.H. Xu, M.Y. Luo, C.L. Zhu, L. Liang, “Removal of aqueous oxalic acid by heterogeneous catalytic ozonation with MnOx/sewage sludge-derived activated carbon as catalysts,” Sci Total Environ, 575 (2017), pp. 50-57

[34]. Yongfei Ma, Ping Li, Lie Yang, Li Wu, Liuyang He, Feng Gao, Xuebin Qi, Zulin Zhang, “Iron/zinc and phosphoric acid modified sludge biochar as an efficient adsorbent for fluoroquinolones antibiotics removal,” Ecotoxicology and Environmental Safety Volume 196, 15 June 2020, 110550

[35] J.Y. Ma, Y. Liu, S. Chen, Y.J. Du, H.F. Wu, “Changes in the pore structure of modified sludge-activated carbon and its effect on the adsorption characteristics of CO2 under high pressure,” Micropor Mesopor Mat, 345 (2022), Article 112255

[36]. G. Ye, J. Zhou, R. Huang, Y. Ke, Y. Peng, Y. Zhou, et al. "Magnetic sludge-based char derived from Fenton sludge as an efficient heterogeneous Fenton catalyst for degrading Methylene blue," Journal of Environmental Chem Eng, vol.10 (2), pp. 107242, 2022.

[37]. Wei Chen, Zhujun Liu, Qian Tang, Bin Du, Xianbin Huang, You Mo, Liangqian Fan, Hongbing Luo, Fenghui Chen, "Assessment of a novel aminated magnetic adsorbent with excellent adsorption capacity for dyes and drugs," Journal of Environmental Management, vol. 293, pp. 112809, 2021.

[38]. S. Li, D. Huang, M. Cheng, Z. Wei, L. Du, G. Wang, S. Chen., L. Lei., Y. Chen., R. Li., "Application of sludge char nanomaterials in Fenton-like processes: Degradation of organic pollutants, sediment remediation, sludge dewatering," Chemosphere, vol. 307, pp. 135873, 2022.

[39] Biswa R. Patra, Sonil Nanda, Ajay K. Dalai, Venkatesh Meda "Taguchi-based process optimization for activation of agro-food waste char and performance test for dye adsorption" Chemosphere, vol. 285, pp. 131531, 2021.

[40]. I. Block, C. Günter., A. D. Rodrigues., S. Paasch., P. Hesemann., $ A. Taubert., "Carbon adsorbents from spent coffee for removal of Methylene blue and methyl orange from water"Materials, vol. 14, pp. 3996, 2021

[41]. Y. wang., H. Li., Y. Shao., H. Guo., Z. Liu., G. Hu., H. Xiang., J. Hu., "Removal of elemental mercury using magnetic Fe-containing carbon prepared from sludge flocculated with ferrous sulfate by Zinc chloride activation," J. of Energ Ins., Vol. 98, pp. 98-106,2021.

[42]. Y.X. Huang., Sun, Y.R.; Xu, Z.H.; Luo, M.Y.; Zhu, C.L.; Li, L. "Removal of aqueous oxalic acid by heterogeneous catalytic ozonation with MnOx/sewage sludge-derived activated carbon as catalysts," Sci. Total Environ, vol. 575, pp. 50–57, 2017.

[43] M.J. Martin, A. Artola, M.D. Balaguer, M. Rigola, "Activated carbons developed from surplus sewage sludge for the removal of dyes from dilute aqueous solutions," Chem. Eng. J., 94 (2003), pp. 231-239

[44] M.A.A. Zaini, M. Zakaria, S.H. Mohd.-Setapar, M.A. Che-Yunus, "Sludge-adsorbents from palm oil mill effluent for methylene blue removal," J. Environ. Chem. Eng., 1 (2013), pp. 1091-1098

[45] H.D. Utomo, X.C. Ong, S.M.S. Lim, G.C.B. Ong, P. Li, "Thermally processed sewage sludge for methylene blue uptake," Int. Biodeter. Biodegrad., 85 (2013), pp. 460-465

[46]. A. T. Bafrooee, H.A. Panahi, E. Moniri, M. Miralinaghi, A.H. Hasani, "Removal of Hg 2+ by carboxyl-terminated hyperbranched poly (amidoamine) dendrimers grafted superparamagnetic nanoparticles as an efficient adsorbent," Environ. Sci. Pollut. Res. pp. 1-21, 2020.

[47]. E. Afshar, M.H. Mohammadi., K.H. Dashti., “Removal of Hg (I) and Hg (II) ions from aqueous solutions, using TiO2 nanoparticles,” Pollution, Volume 3(3), pp. 505-516,2017.

[48]. A. Bahiraei, J. Behin, “Sonochemical immobilization of MnO_2 nanoparticles on NaP-zeolite for enhanced Hg (II) adsorption from water,” J. Environ. Chem. Eng., 83 (2020), Article 103790

[49]. E.E. Congdon, et al., Methylthioninium chloride (methylene blue) induces autophagy and attenuates tauopathy in vitro and in vivo, Autophagy 8 (4) (2012) 609–622.

[50] Programme, U.N.E., 2018. Global Mercury Assessment.

[51] F. Wang., S. Wang., L. Zhang., H. Yang., W. Gao., Q. Wu., J. Hao., “Mercury mass flow in iron and steel production process and its implications for mercury emission control,” J. Environ. Sci. (China) 43, 293–301, 2016.

[52] K. Kogut., J. Gorecki., P. Burmistrz., “Opportunities for reducing mercury emissions in the cement industry. J. Clean. Prod. 293, 126053, 2021.

[53]. Wu, Qingru, Li, Guoliang, Wang, Shuxiao, Liu, Kaiyun, Hao, Jiming, “Mitigation Options of Atmospheric Hg Emissions in China,” Environ. Sci. Technol. 52 (21), 12368–12375, 2018.

[54]. Charv´ at, P., Klimeˇs, L., Pospíˇsil, J., Klemeˇs, J.J., Varbanov, P.S., “An overview of mercury emissions in the energy industry-A step to mercury footprint assessment,” J. Clean. Prod. 267, 122087, 2020.

[55]. F. Beckers., J. Rinklebe., “Cycling of mercury in the environment: sources, fate, and human health implications: a review,” Crit. Rev. Environ. Sci. Technol, 47, 693–794, 2017.

[56]. Q. Zhang, J. Chang, T. Wang, et al. “Review of biomass pyrolysis oil properties and upgrading research,” Energy Convers Manage, Vol. 48, pp. 87–92, (2007).

[57]. O. Tursunov., B. Suleimenova., B. Kuspangaliyeva., V.J. Inglezakis., E.J. Anthony., Y. Sarbassov," Characterization of tar generated from the mixture of municipal solid waste and coal

pyrolysis at 800 ◦C," Energy Reports 6, pp. 147–152, 2020.

[58]. D. Kalampaliki, G.D.T.M. Jayasinghe, E. Avramiotis, I.D. Manariotis, D. Venier, S.G. Poulopoulos, J. Szpunar, J. Vakros, D. Mantzavinos, "Application of KOH-activated char for the activation of persulfate and the degradation of sulfamethoxazole,2023. DOI: https://doi.org/10.1016/j.cherd.2023.04.056

[59] Direct determination (analysis) of mercury in coal by ASTM D6722-11 and EPA 7473 (lumexinstruments.com)

[60] US EPA, SW-846, Method 6010C, Inductively Coupled Plasma-Atomic Emission Spectrometry, US EPA 6010, 2007.

[61]. Y. Zhai, W. Peng, G. Zeng, Z. Fu, Y. Lan, H. Chen, C. Wang, X. Fan, Pyrolysis characteristics and kinetics of sewage sludge for different sizes and heating rates, J. Therm. Anal. Calorim. 107, pp. 1015–1022, 2012.

[62]. D. V. Suriapparao, R. Vinu, “Effects of Biomass Particle Size on Slow Pyrolysis Kinetics and Fast Pyrolysis Product Distribution,” Waste Biomass Valor, 2017. DOI 10.1007/s12649-016-9815-7

[63]. Li. Binbin, S. Ding., H. Fan., Yu Ren., "Experimental Investigation into the effect of pyrolysis on chemical forms of heavy metals in sewage sludge char (SSB), with Brief Ecological Risk Assessment, Materials, vol. 14(2), pp. 447, 2021.

[64]. Zhang, J., Lü, F., Zhang, H., Shao, L., Chen, D., He, P., 2015. Multiscale visualization of sewage sludge biochar's structural and characteristic changes is oriented toward potential agronomic and environmental implications. Sci. Rep. 5, 1–8. https://doi. org/10.1038/srep09406.

[65]. P. Zhang, Y. Li, Y. Cao, L. Han, “Characteristics of tetracycline adsorption by cow manure biochar prepared at different pyrolysis temperatures,” Bioresource. Technol., Vol. 285, pp.

121348, 2019.

[66]. H. Liu., G. Xu., G. Li., “The characteristics of pharmaceutical sludge-derived char and its application for the adsorption of tetracycline,” Science of The Total Environment, Vol. 747, pp. 141492, 2020.

[67]. A. Zielińska, P. Oleszczuk, “The conversion of sewage sludge into biochar reduces polycyclic aromatic hydrocarbon content and ecotoxicity but increases trace metal content,” Biomass Bioenergy, 75 (2015), pp. 235-244

[68]. H. Peng, P. Gao, G. Chu, B. Pan, J. Peng, B. Xing, “Enhanced adsorption of Cu (II) and Cd (II) by phosphoric acid-modified biochars,” Environ. Pollut. 229 (2017), pp. 846-853

[69]. X.Q. Liu, H.S. Ding, Y.Y. Wang, W.J. Liu, H. Jiang, “Pyrolytic temperature dependent and ash catalyzed formation of sludge char with ultra-high adsorption to 1-naphthol,” Environ. Sci. Technol., 50 (2016), pp. 2602-2609

[70]. Raj A., Yadav A., Arya S., Sirohi R., Kumar S., Rawat A. P., Thakur R. S., Patel D. K., Bahadur L., Pandey A., “Preparation, characterization and agri applications of biochar produced by pyrolysis of sewage sludge at different temperatures,” Science of The Total Environment Volume 795, 2021, 148722

[71]. A. Nematollahzadeh, S. Seraj, B. Mirzayi, “Catecholamine-coated maghemite nanoparticles for the environmental remediation: hexavalent chromium ions removal. Chem. Eng. J. 277, 21e29, 2015.

[72]. M. Khraisheh, M. Al-Ghouti, S. Allen, M. Ahmad, Effect of O.H. and silanol groups in removing dyes from aqueous solution using diatomite, Water Res., Vol. 39, pp. 922–932, 2005.

[73]. Zhang, P., O'Connor, D., Wang, Y., Jiang, L., Xia, T., Wang, L., Tsang, D.C.W., Ok, Y.S., Hou, D., "A green char/iron oxide composite for methylene blue removal," J. Hazard. Mater, Vol. 384, pp. 121286, 2020. https://doi.org/10.1016/j.jhazmat.2019.121286.

[74]. B. Obradovic, 2020. Guidelines for general adsorption kinetics modeling. Hem. Ind. Doi: 10. 2298/HEMIND2002010060

.

[75]. Y. Sun, C. Ding, W. Cheng, X. Wang, Simultaneous adsorption, and reduction of U (VI) on reduced graphene oxide-supported nanoscale zerovalent iron, J. Hazard. Mater, Vol. 280, pp. 399–408, 2014.

[76]. L. Gu., N. Zhu, H. Guo, S. Huang, Z., Lou, H. Yuan., "Adsorption and Fenton-like degradation of naphthalene dye intermediate on sewage sludge derived porous carbon," J. of Hazard. Mat., Vol. 246(247), pp. 145 -153, 2013.

[77]. S. Fana., Y. Wanga., Z. Wanga., J. Tanga., J. Tanga., X. Lia," removal of methylene blue from aqueous solution by sewage sludge-derived biochar: Adsorption kinetics, equilibrium, thermodynamics, and mechanism", J. of Environ. Chem. Eng., Vol. 5, pp. 601–611, 2017.

[78]. F.C. Wu, R.-L. Tseng, R.-S. Juang, "Characteristics of Elovich equation used to analyze adsorption kinetics in dye-chitosan systems," Chem. Eng. J., Vol.150, pp. 366–373, 2009.

[79] D. Mitrogiannis, G. Markou, A. Çelekli, H. Bozkurt, “Biosorption of methylene blue onto Arthrospira platensis biomass: kinetic, equilibrium and thermodynamic studies,” J. Environ. Chem. Eng. Vol. 3, pp. 670–680, 2015.

[80] H. Lu, W. Zhang, S. Wang, L. Zhuang, Y. Yang, R. Qiu, “Characterization of sewage sludge-derived biochars from different feedstocks and pyrolysis temperatures,” J. Anal. Appl. Pyrolysis, Vol. 102, pp. 137–143, 2013.

[81] L. Leng, X. Yuan, H. Huang, J. Shao, H. Wang, X. Chen, G. Zeng, “Bio-char derived from sewage sludge by liquefaction: characterization and application for dye adsorption,” Appl. Surf. Sci. Vol. 346, pp. 223–231, 2015.

[82] L. Shi, G. Zhang, D. Wei, T. Yan, X. Xue, S. Shi, Q. Wei, “Preparation and utilization of anaerobic granular sludge-based biochar for the adsorption of methylene blue from aqueous solutions,” J. Mol. Liq. Vol.198, pp. 334–340, 2014.

[83]. C. A. Takaya., L. A. Fletcher., S. Singh., K. U. Anyikude, & A. B Ross., “Phosphate and ammonium sorption capacity of biochar and hydrochar from different wastes,” *Chemosphere, Vol.* 145, pp. 518–527, 2016.

[84] H. Wang., R. Duan., X. Zhou., J. Wang., Y. Liu., R. Xu., “Efficient removal of mercury and chromium from wastewater *via* biochar fabricated with steel slag: Performance and mechanisms,” Bioprocess Eng. Vol.10, 2022.

[85] H. Wang., Y. Liu., J. Ifthikar., L. Shi., A. Khan., & Z. Chen., “Towards A better understanding on mercury adsorption by magnetic bio-adsorbents with gamma-Fe_2O_3 from pinewood sawdust derived hydrochar: Influence of atmosphere in heat treatment,” *Bioresour. Technol. Vol.* 256, pp. 269–276, 2018.

[86]. J. Hoslett, H. Ghazzal, N. Mohamad, H. Johura, “Removal of methylene blue from aqueous solutions by char prepared from the pyrolysis of mixed municipal discarded material,” Sci. Total Environ. (2020), p. 136832

[87]. R. Ismaturrahmi, I. Mustafa, “Methylene blue removal from water using H2SO4 crosslinked magnetic chitosan nanocomposite beads, “Microchem. J., 144, pp. 397-402, 2019.

[88] L. Mouni, L. J.C Belkhiri., A. Bollinger, B. A. Assadi, A. Tirri, F. Dahmoune, K. Ma dani, H. Remini, “Removal of methylene blue from aqueous solutions by adsorption on kaolin: kinetic and equilibrium studies,” Appl. Clay Sci., 153, pp. 38-45, 2018.

[89]. Xu X, Schierz A, Xu N, Cao X (2016) Comparison of the characteristics and mechanisms of Hg (II) sorption by chars and activated carbon. J Colloid Interface Sci 463:55–60

[90]. Lu X, Jiang J, Sun K, et al. (2014) Influence of the pore structure and surface chemical properties of activated carbon on the adsorption of mercury from aqueous solutions. Mar Pollut Bull 78:69–76

[91]. Rao MM, Reddy DHKK, Venkateswarlu P, Seshaiah K (2009) Removal of mercury from aqueous solutions using activated carbon prepared from agricultural byproduct/waste. J Environ Manag 90:634–643

[92]. Tan G, Sun W, Xu Y et al. (2016) Bioresource technology sorption of mercury (II) and atrazine by char, modified chars and char-based activated carbon in aqueous solution. Bioresour Technol 211:727–735

APPENDICES

A. Appendices for Chapter 3

Fig A1. Location of Sewage Sludge Treatment Facility

Fig A2. Flowchart of the Preparation of Municipal Sewage Sludge

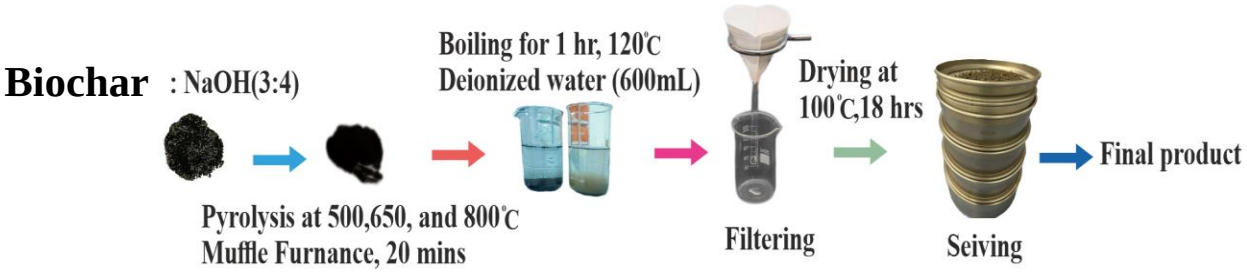

Fig A3. Flowchart of Synthesis of Modified Biochar (MS_3)

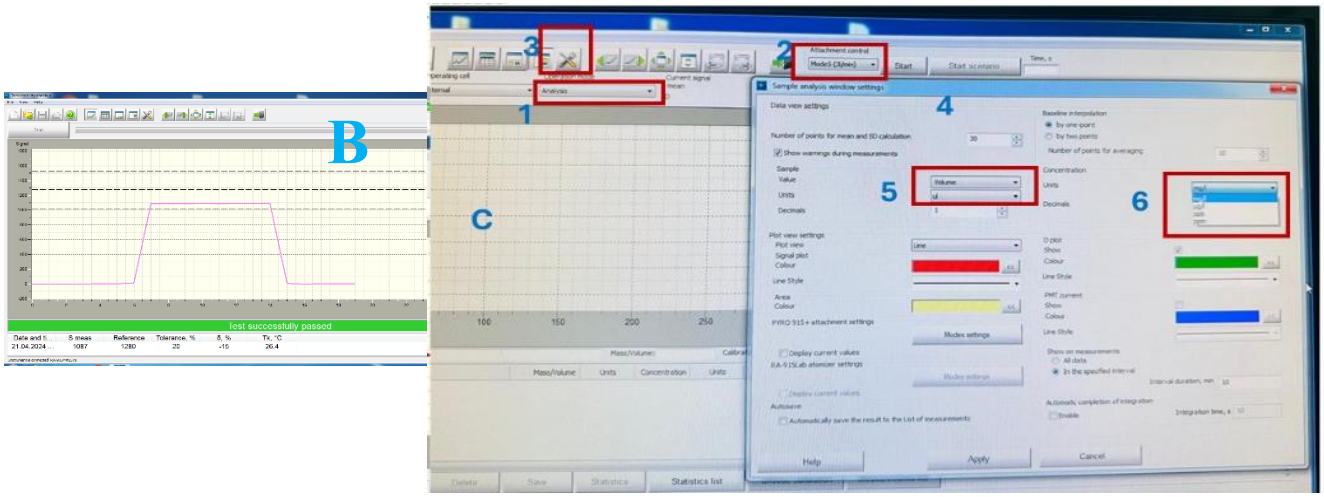

Fig A4 Shows the operations of the Mercury Analyzer

Step 1: Turn on the system Units and the monitor, and then Enter the password

Step 2: Turn on the analyzer and the pumping Units

Step 3: Open the Rapid software and enter the password

Step 4: Run a serviceability check (Shown in Fig B) to see if the optical lens is in good condition. If not, you must open the optical units, change the filter dust, or clean the lens.

Step 6: Go to operation mode(number 1) and select calibration or analysis

Step 7: Go to attachment control and select the type of mode(For mercury mode 5 and coal

analysis mode 7). Mode 5 has a flow rate of 3L/min and an operating temperature of 750 °C. (Inbuilt function). Note: Oxygen is used for pyrolysis.

Step 8: Go to the mode settings shown as number 3; the template labeled 4 will appear.

Step: Go to number 5 and select the unit of the volume of adsorbate to deliver. (eg, 20 µL)

Step 9: Go to number 6, select the units of your measurement either for calibration or analysis and click apply when done

Step 10: Click on the start button and allow a period of 15 minutes for the system to equilibrate (achieve stable peaks and voltage)

Step 11: Find Mass/Volume, and insert the volume of adsorbate to deliver. The system will consider all these to calculate the mercury concentration.

Table A5 Assay of Chemicals Used for Study

Chemical Reagent	Purity (%)	Molar Weight (g/mol)	Density (g/cm3)	CAS Number
HNO3	>=69.0%	63.01	1.420	7697-37-2
HCL	>=37.0%	36.46	1.190	7647-01-0
HCLO4	65-71%	100.46	2.4994	7601-90-3
HF	>=48.0%	20.01	1.170	7664-39-3
H3BO3	99.9	61.83	1.44	10043-35-3
Methylene Blue	>70%	319.85	1.230	61-73-4
Mercury	99%	324.7	4.3	10045-95-0

B. Appendices of Chapter 4

Table B1. Other elements in raw SS, and SS-derived biochar at different temperatures and different sized fraction

	Raw Municipal Sewage Sludge							
Particle size	**Ca**	**Si**	**Mg**	**Na**	**K**	**Ti**	**Pb**	**Co**
S_1	27.76± 0.013	70± 0.37	4.59± 0.01	1.71± 0.001	3.46± 0.01	1.13± 0.00	0.04± 0.00	0.001 ± 0.00
S_2	27.29± 0.04	72± 0.03	4.43± 0.01	1.72± 0.003	3.09± 0.01	1.13± 0.00	0.05± 0.00	0.01± 0.00
S_3	25.78± 0.01	**71± 0.01**	4.4± 0.01	1.63± 0.000	3.33± 0.03	1.03± 0.00	0.05± 0.00	0.005± 0.00
S_4	30.14± 0.01	70± 0.01	5.69± 0.002	1.82± 0.000	3.07± 0.02	1.08± 0.00	0.05± 0.00	0.01± 0.00
	Sewage sludge-derived Biochar at 500 °C							
S_1	43.00±0.01	145± 0.34	6.57 ± 0.01	4.46± 0.001	6.86± 0.001	5.9± 0.00	0.1 ± 0.00	0.02 ± 0.00
S_2	37.00±0.01	155± 0.42	6.42± 0.005	3.61± 0.001	7.82 ± 0.03	2.36± 0.01	0.1 ± 0.00	0.01 ± 0.00
S_3	35.00±0.06	**184± 0.16**	7.91 ± 0.01	5.07 ± 0.01	10.2 ± 0.03	3.1± 0.00	0.13 ± 0.00	0.02 ± 0.00
S_4	40.00±0.13	169± 0.38	7.69± 0.003	4.25± 0.002	8.43± 0.002	2.5± 0.00	0.12 ± 0.00	0.01 ± 0.00
	Sewage sludge-derived Biochar at 650 °C							
S_1	38.00±0.04	176± 0.3	6.40± 0.002	4.24± 0.001	9.25± 0.013	2.7± 0.0	0.12 ± 0.00	0.02 ± 0.00
S_2	27.00±0.001	140± 0.1	5.19± 0.001	3.23± 0.001	6.93± 0.001	2.1± 0.00	0.09 ± 0.00	0.01 ± 0.00
S_3	43.00±0.02	**175± 0.44**	6.94± 0.011	4.73 ± 0.01	9.86 ± 0.03	2.8± 0.00	0.12 ± 0.00	0.02 ± 0.00
S_4	42.00±0.05	175± 0.17	8.05± 0.003	4.55± 0.001	9.01 ± 0.02	2.7± 0.00	0.12 ± 0.00	0.01 ± 0.00
	Sewage sludge-derived Biochar at 800 °C							
S_1	20.80±0.03	52± 0.1	3.53±0.00	2.02±0.00	3.66±0.00	1.3± 0.00	0.08±0.00	0.01±0.00
S_2	21.08±0.01	68± 0.125	5.63±0.01	2.85±0.00	5.16±0.00	1.8± 0.00	0.11±0.00	0.01±0.00
S_3	17.58±0.02	**40± 0.04**	4.04±0.00	1.83±0.00	3.33±0.00	1.14± 0.00	0.07±0.00	0.01±0.00
S_4	44.46±0.04	85± 0.03	8.41±0.00	3.52±0.00	6.11±0.01	2.1± 0.00	0.14±0.00	0.03±0.00

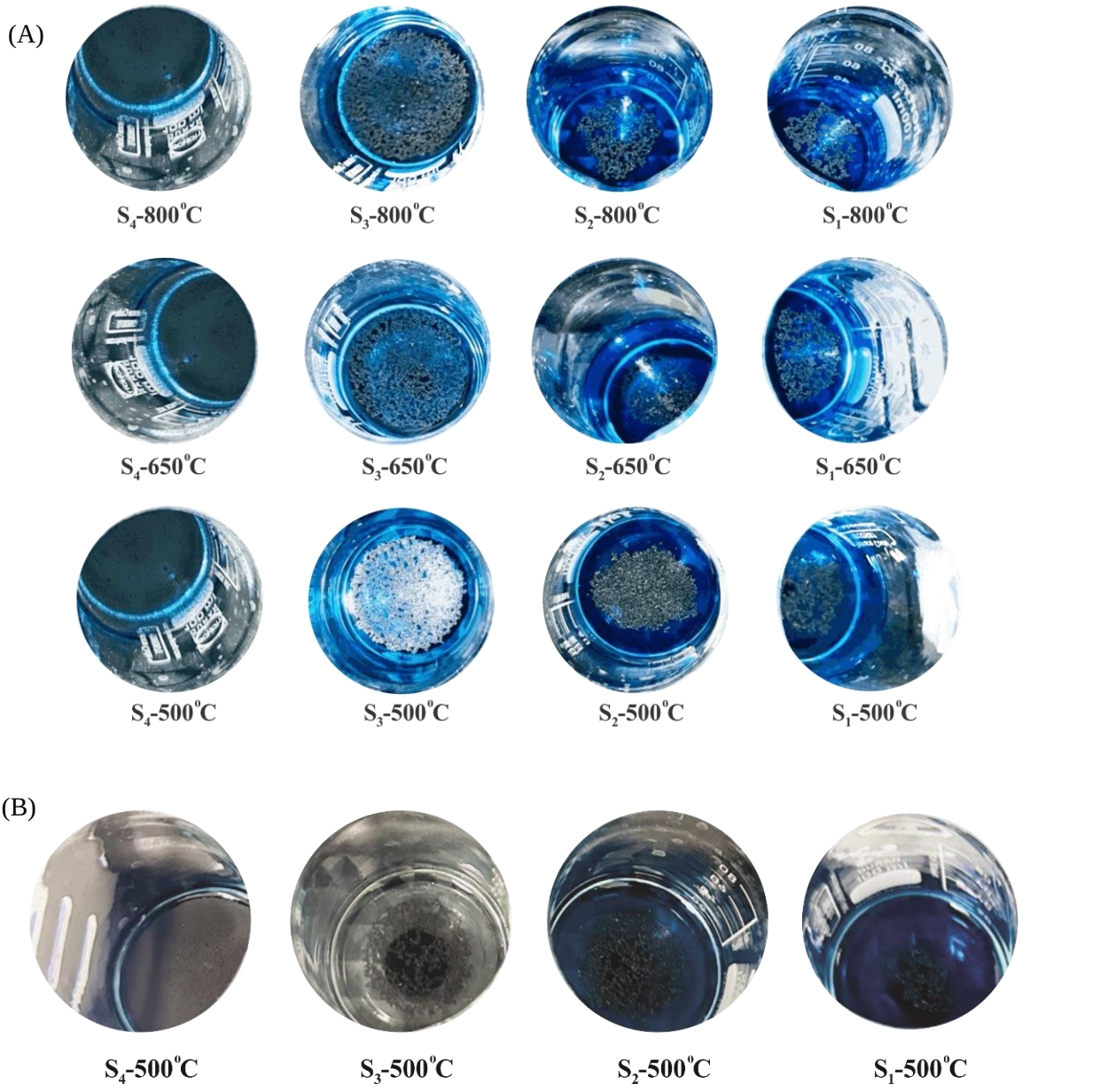

Fig B2, Physical Nature of sewage sludge-derived biochar pyrolyzed at 500 °C, 650 °C and 800 °C During MB Adsorption(A) and at the Equilibrium Stage(B) (Adsorbent dose: 30 mg, Co: 10 mg/L MB, pH: 6.5, rpm: 150rev/min)

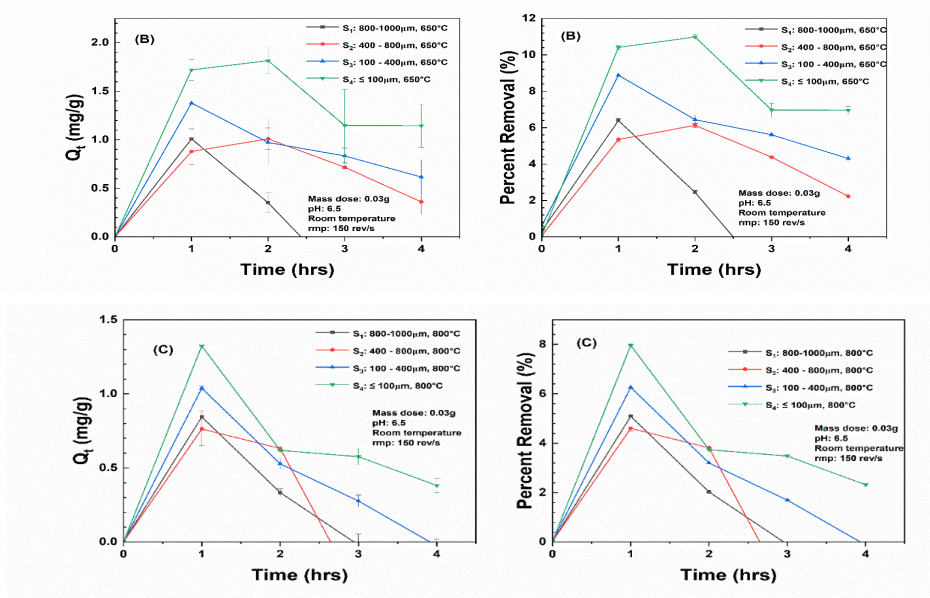

Fig. B3: Adsorption Capacity of SS-derived Biochar at 650 °C (B) and at 800 °C (C) versus Time (10 ppm MB, Adsorbent mass: 30 mg, pH of 6.5 at 25 °C, oscillating speed at 150 rpm).

Table B4: The fit parameters for adsorption of 10 mg/L of MB over different particles sized SS biochar for Pseudo first-order kinetics model, Pseudo second-order kinetics model, Webber-Morris Model and Elovich Model, along with the corresponding R^2.

SS-biochar particle size	Kinetic Parameters Pseudo 1st Order				Kinetic Parameters Pseudo 2nd Order			
	Calc Q_e (mg/g)	Exp Q_e (mg/g)	k_1	R^2	Calc Q_e (mg/g)	Exp Q_e (mg/g)	k_2	R^2
S_1 – 500 °C	5.00	5.7	0.015	0.93	5.6	5.7	0.004	0.94
S_2 – 500 °C	3.7	3.6	0.030	0.90	3.7	3.7	0.028	0.89
S_3 – 500 °C	14	15	0.005	0.96	17	15	0.0003	0.97
S_4 – 500 °C	10	11	0.008	0.94	12	11	0.0007	0.95

SS-biochar particle size	Webber-Morris model			Elovich Model		
	K_d	C	R^2	α	β	R^2
S_1 – 500 °C	0.19	1.12	0.83	0.57	1.10	0.94
S_2 – 500 °C	0.10	1.50	0.50	1.81	8.71	0.89
S_3 – 500 °C	0.58	0.80	0.99	0.17	0.22	0.99
S_4 – 500 °C	0.44	0.90	0.95	0.19	0.35	0.97